

## Secondary organic aerosol formation from fossil fuel sources contribute majority of summertime organic mass at Bakersfield

Shang Liu,<sup>1,2</sup> Lars Ahlm,<sup>1</sup> Douglas A. Day,<sup>1,3</sup> Lynn M. Russell,<sup>1</sup> Yunliang Zhao,<sup>4</sup> Drew R. Gentner,<sup>5</sup> Robin J. Weber,<sup>4</sup> Allen H. Goldstein,<sup>4,5</sup> Mohammed Jaoui,<sup>6</sup> John H. Offenberg,<sup>7</sup> Tadeusz E. Kleindienst,<sup>7</sup> Caitlin Rubitschun,<sup>8</sup> Jason D. Surratt,<sup>8</sup> Rebecca J. Sheesley,<sup>9</sup> and Scott Scheller<sup>10</sup>

Received 22 May 2012; revised 31 August 2012; accepted 9 October 2012; published 15 December 2012.

[1] Secondary organic aerosols (SOA), known to form in the atmosphere from oxidation of volatile organic compounds (VOCs) emitted by anthropogenic and biogenic sources, are a poorly understood but substantial component of atmospheric particles. In this study, we examined the chemical and physical properties of SOA at Bakersfield, California, a site influenced by anthropogenic and terrestrial biogenic emissions. Factor analysis was applied to the infrared and mass spectra of fine particles to identify sources and atmospheric processing that contributed to the organic mass (OM). We found that OM accounted for 56% of submicron particle mass, with SOA components contributing 80% to 90% of OM from 15 May to 29 June 2010. SOA formed from alkane and aromatic compounds, the two major classes of vehicle-emitted hydrocarbons, accounted for 65% OM (72% SOA). The alkane and aromatic SOA components were associated with 200 nm to 500 nm accumulation mode particles, likely from condensation of daytime photochemical products of VOCs. In contrast, biogenic SOA likely formed from condensation of secondary organic vapors, produced from NO<sub>3</sub> radical oxidation reactions during nighttime hours, on 400 nm to 700 nm sized primary particles, and accounted for less than 10% OM. Local petroleum operation emissions contributed 13% to the OM, and the moderate O/C (0.2) of this factor suggested it was largely of secondary origin. Approximately 10% of organic aerosols in submicron particles were identified as either vegetative detritus (10%) or cooking activities (7%), from Fourier transform infrared spectroscopic and aerosol mass spectrometry measurements, respectively. While the mass spectra of several linearly independent SOA components were nearly identical and external source markers were needed to separate them, each component had distinct infrared spectrum, likely associated with the source-specific VOCs from which they formed.

**Citation:** Liu, S., et al. (2012), Secondary organic aerosol formation from fossil fuel sources contribute majority of summertime organic mass at Bakersfield, *J. Geophys. Res.*, 117, D00V26, doi:10.1029/2012JD018170.

### 1. Introduction

[2] The organic fraction of atmospheric particles is composed of a complex mixture of thousands of individual compounds [Hamilton *et al.*, 2004], which originate from a variety of sources and processes. In urban areas, the major

source is fossil fuel combustion from gasoline- and diesel-powered vehicles and other industrial activities (e.g., oil burning). Emissions from these sources are largely composed of alkane and aromatic hydrocarbons, with a minor fraction of alkene compounds [Kirchstetter *et al.*, 1999; Schauer

<sup>1</sup>Scripps Institution of Oceanography, University of California, San Diego, La Jolla, California, USA.

<sup>2</sup>Now at Los Alamos National Laboratory, Los Alamos, New Mexico, USA.

<sup>3</sup>Now at Cooperative Institute for Research in Environmental Studies, University of Colorado Boulder, Boulder, Colorado, USA.

Corresponding author: L. M. Russell, Scripps Institution of Oceanography, University of California, San Diego, La Jolla, CA 92037, USA. (lmrusse@ucsd.edu)

This paper is not subject to U.S. copyright.

Published in 2012 by the American Geophysical Union.

<sup>4</sup>Department of Environmental Science, Policy and Management, University of California, Berkeley, California, USA.

<sup>5</sup>Department of Civil and Environmental Engineering, University of California, Berkeley, California, USA.

<sup>6</sup>Alion Science and Technology, Research Triangle Park, North Carolina, USA.

<sup>7</sup>National Exposure Research Laboratory, U.S. EPA, Research Triangle Park, North Carolina, USA.

<sup>8</sup>Department of Environmental Sciences and Engineering, Gillings School of Global Public Health, University of North Carolina at Chapel Hill, Chapel Hill, North Carolina, USA.

<sup>9</sup>Department of Environmental Science, Baylor University, Waco, Texas, USA.

<sup>10</sup>California Air Resources Board, Sacramento, California, USA.

*et al.*, 1999]. Another important source, biogenic emissions, accounts for 90% of total volatile organic compounds (VOCs) globally [Goldstein and Galbally, 2007] and is key to particle formation in some regions (e.g., the southeastern U.S.) [Goldstein *et al.*, 2009]. After emission, VOCs are transported from their sources during which time they are oxidized in the atmosphere, forming low-volatility products that can condense into the particle phase. The organic aerosols formed in the atmosphere are categorized as “SOA” (secondary organic aerosol) as opposed to “POA” (primary organic aerosols), which are directly emitted at their sources.

[3] Formation of SOA is a dynamic process that involves complex chemical reactions and physical transformations. Despite significant progress in the past years, quantitative measurement of SOA mass and its mass fraction in organic aerosols remains challenging. The elemental carbon (EC) tracer analysis has been used to identify non-SOA components since the 1980s [Grosjean, 1984]: The organic carbon (OC)-to-EC ratio that exceeds the average OC/EC from source measurements is assumed to be SOA [Turpin *et al.*, 1991]. Using this method, field measurements conducted at Los Angeles suggested that production of SOA could be 3 to 4 times more than that of POA during smog events [Grosjean, 1984; Turpin *et al.*, 1991]. Supporting the argument that SOA could be the major OM component were reaction chamber studies carried out during this time, which showed high mass yields of precursor compounds [Hatakeyama *et al.*, 1985, 1987]. However, the EC tracer approach suffers from large uncertainties, since OC/EC of emission sources is highly variable and is substantially affected by meteorological conditions (e.g., air mixing) [Gray *et al.*, 1986]. Another approach, the organic tracer-based chemical mass balance (CMB) model [Schauer *et al.*, 1996; Cass, 1998], has been applied to identify sources of atmospheric fine particles since the 1990s. In this method, the mass that cannot be predicted by the model is assigned to SOA [Schauer *et al.*, 2002a; Zheng *et al.*, 2002]. Therefore, the CMB model does not directly predict SOA but provides an upper limit of SOA mass based on limited source markers (source types) [Cass, 1998]. Over the last 10 years, the development of aerosol mass spectrometer (AMS) and Fourier transform infrared (FTIR) spectroscopy has provided new insights for SOA quantification [Jayne *et al.*, 2000; Maria *et al.*, 2002]. Positive matrix factor (PMF) analysis applied to the AMS and FTIR measurements during field experiments carried out worldwide consistently showed that 65% to 95% of OM is oxygenated organic aerosols (OOA), having higher OM/OC and oxygen-to-carbon molar ratio (O/C) composition than expected for primary organic components [Jimenez *et al.*, 2009; Lanz *et al.*, 2007; Liu *et al.*, 2011; Russell *et al.*, 2011; Russell, 2003; Turpin *et al.*, 2000; Zhang *et al.*, 2007].

[4] However, there is a lack of direct evidence that oxidized OA equates to SOA, because some primary aerosols are oxidized (e.g., marine polysaccharides and vegetative detritus). Consequently, there is a need to directly compare OOA to laboratory-produced SOA. Russell *et al.* [2011] compared OOA to SOA generated in a smog chamber. In this case, OOA was derived by factor analysis of FTIR measurements, a technique that provides more molecular functional group specificity than mass spectra methods that employ electron ionization. Results of this comparison suggested that functional group compositions of OOA and SOA are comparable and precursor (and sometimes oxidant)

dependent, making it possible to separate out SOA and, so, help address the controversy of POA and SOA mass fractions. In addition, Russell *et al.* [2011] proposed that atmospheric alkanes are important SOA precursors—oxidation of alkanes produces multigeneration SOA products, which is supported by a recent model simulation study [Yee *et al.*, 2012] that suggests more than two thirds of alkane SOA are fourth-generation or higher products after reaction for 10 h. Despite the improvements in laboratory and model studies, more field measurements are needed to separate SOA formed from different precursors and identify which mechanisms best explain chemical properties of SOA formed in the complex atmosphere.

[5] Size distributions of SOA components can provide additional insights for identifying source and formation mechanisms of ambient particles. Primary combustion-related particles, such as those emitted from gasoline- and diesel-powered vehicles, are typically smaller than 100 nm [Kittelson, 1998], whereas dust particles are usually larger than 500 nm [Tegen and Lacis, 1996]. Primary particles from cooking activities, including charbroiling and frying, are found to be smaller than 200 nm [Wallace *et al.*, 2004]. Particles in 200 nm to 500 nm size range typically contain SOA formed by condensation of secondary organic vapors, because particles in this size range have the highest relative surface area that make mass transfer most efficient for growth [Maria *et al.*, 2004; Seinfeld and Pandis, 2006]. Size distributions of organic components are also important for evaluating climate impacts of aerosols, since radiative parameters of aerosol particles are strongly dependent on particle size [Tegen and Lacis, 1996]. Further, lifetime of particles, which determines the distance that particles can travel and hence particles' regional impacts, is affected by particle size. For these reasons, particle size distributions have been studied extensively [Heintzenberg *et al.*, 2000; Hoppel *et al.*, 1990; Whitby *et al.*, 1972]. Although some specific SOA molecules (e.g., oxalic acid) or mass fragments (e.g.,  $m/z$  44) have been measured as functions of size [Kawamura *et al.*, 2007; Alfarra *et al.*, 2004], predicting size distributions of different types of ambient SOA (formed from different sources or processes) is challenging. A few studies have applied factor analysis to each size fraction of size-resolved filter measurements (2–6 size ranges) with limited organic mass quantification [Han *et al.*, 2006; Karanasiou *et al.*, 2009; Richard *et al.*, 2011; Srivastava *et al.*, 2008]. In these studies, estimates of factor size distribution were made by comparing masses of the common factors (typically representing primary sources) derived from each size fraction. However, this approach is not practical for highly size-resolved data sets (e.g., AMS measurements with more than 100 size bins). Another approach, 3-D factorization method, has been valuable for providing time-resolved size distribution of factors and has been recently applied to AMS measurements with success [Ulbrich *et al.*, 2012]. However, to generate physically meaningful factors, this analysis often requires prior information derived from 2-D factorization plus comparisons of results derived from different 3-D factorization methods, which is complicated and, so, the 3-D factorization methods have not been widely used. Thus, despite these improvements, size distributions of ambient SOA components have not been widely investigated.

[6] In this context, we used collaborative measurements at Bakersfield in the San Joaquin Valley (SJV), one of the

most polluted regions in the United States [Chow *et al.*, 1996], to study the oxidized fraction of OM. We began by quantifying oxygenated organic functional group and mass fragment abundances of bulk and single particles. Next, we identified sources and processes that contributed to OM using factor analysis and source-specific organic and inorganic marker compounds. After distinguishing secondary components from primary emissions, we evaluated the SOA fraction of OM. In addition, primary and secondary single-particle types were identified using cluster analysis. Finally, we compared different secondary organic components—their precursors, oxidants that lead to formation, and time of production. Size distributions of the SOA components were used to help identify their potential formation mechanisms. These analyses were built on a set of particle- and gas-phase measurements presented below.

## 2. Experimental Setup

### 2.1. Sampling Site and Meteorological Conditions During the CalNex Campaign

[7] The California Research at the Nexus of Air Quality and Climate Change (CalNex) campaign is a collaborative effort aimed at characterizing chemical and physical properties of gases and aerosols in California. One of the two CalNex supersites was located near Bakersfield in Kern County in the San Joaquin Valley (SJV). The SJV is surrounded by coastal mountain ranges to the west, the Sierra Nevada range to the east, and the Tehachapi Mountains to the south [Chow *et al.*, 2006b], topography that regularly precludes air ventilation. The basin's air pollution levels are especially high during wintertime [Chow *et al.*, 2006a, 2006b]. Bakersfield, located in the southern portion of the SJV and one of its biggest cities, has wintertime PM<sub>2.5</sub> concentrations that often exceed 50  $\mu\text{g m}^{-3}$ , with OM typically accounting for more than 50% of the PM<sub>2.5</sub> mass [Chow *et al.*, 2006b]. Previous studies conducted at other sites in Bakersfield showed that gasoline- and diesel-powered vehicles, wood combustion, and meat cooking comprise the city's major air pollution sources [Kleeman *et al.*, 2009; Schauer and Cass, 2000] with wood combustion prevailing only in winter [Chow *et al.*, 2006b]. In addition, biogenic hydrocarbons emitted from trees in the foothills are likely significant contributors to summertime VOCs [Tanner and Zielinska, 1994], which are potential precursors to form biogenic SOA. Thus, the high concentration of air pollution and the variety of its sources make Bakersfield an ideal site for studying ambient particles.

[8] Measurements were conducted in association with CalNex from 15 May to 29 June 2010 at Bakersfield (35.35°N, 118.97°W). The sampling site was located on the southeast edge of the urban area near Highway 99 (7 km to the west) and Highway 58 (0.8 km to the north) and had no nearby obstructions (e.g., tall trees or buildings). Instruments were deployed in temperature-controlled (20°C) containers with sampling heights of 3 to 5 m and 18 to 20 m above ground level, respectively, for particle-phase and gas-phase measurements. The sampling period was characterized by a series of clear, dry days with consistent diurnal cycles of temperature and relative humidity (RH), except for 15 to 17 May when intermittent rainfall occurred. The average temperature for the campaign, 24°C, included a 7°C standard deviation, with minimums typically occurring at ~0500 h and

maximums often occurring at ~1500 h (lagging peak solar radiation by 3 h). RH was anticorrelated with temperature, with an average of 38% and a standard deviation of 17%. The observed diurnal cycle of wind direction was consistent with the pattern described by Zhong *et al.* [2004]: Northwesterly winds prevailed during daytime (0800 to 2100 h); between midnight and early morning, easterly and southeasterly winds prevailed for 34 (of 45) days. Easterly and southeasterly winds represented downslope flows [Zhong *et al.*, 2004] that likely included biogenic VOCs emitted from the mountains' coniferous trees (e.g., Sequoia National Forest). The chemistry of these air masses were distinct from the anthropogenic pollutants (e.g., aromatic and alkane hydrocarbons) associated with the predominant northwesterly airflow.

## 2.2. Spectroscopic Measurements

### 2.2.1. Bulk Particle Organic Functional Groups

[9] PM<sub>1</sub> and PM<sub>2.5</sub> filter (Teflon filters with pore size of 1  $\mu\text{m}$ ) samples were collected for FTIR analysis. Five PM<sub>1</sub> samples were collected daily, representing morning (0600–1200 h), early afternoon (1200–1500 h), late afternoon (1500–1800 h), evening (1800–2300 h), and nighttime (0000–0600 h) periods (local time is used throughout the text). The improved time resolution of FTIR PM<sub>1</sub> samples (compared to previously reported 12 or 24 h samples in Russell *et al.* [2011]) allows analysis of diurnal variations of organic functional groups. Shorter sampling times also greatly enhanced statistical significance of data analysis (e.g., correlation analysis) and reduced uncertainties caused by loss of semivolatiles compounds. The single PM<sub>2.5</sub> sample collected each day (0000–2300 h) that overlapped the multiple PM<sub>1</sub> sample collection times characterized the daily average PM<sub>2.5</sub> concentration. Sample preparation and postprocessing have been detailed previously [Gilardoni *et al.*, 2009; Liu *et al.*, 2009]. Briefly, the filters were scanned using a Bruker Tensor 27 FTIR spectrometer with a deuterated triglycine sulfate (DTGS) detector (Bruker, Waltham, MA) before and after sample collection. Collected samples were immediately stored in a freezer (<0°C). An automated algorithm was used to conduct background subtraction, spectrum baselining, peak fitting, and peak integration procedures [Day *et al.*, 2010; Russell *et al.*, 2009]. Mass concentrations of organic functional groups, including alkane, hydroxyl, carboxylic acid, amine, carbonyl, organonitrate, alkene, aromatic, and organosulfate groups, were quantified. Alkene and aromatic groups were below detection limit of the FTIR measurements for all samples, likely because the majority of these groups were oxidized to form SOA components that do not contain C=C bond. Therefore, alkane and aromatic groups were excluded from this study.

### 2.2.2. Single-Particle Microscopy of Organic Functional Groups

[10] Single particles were impacted on Si<sub>3</sub>N<sub>4</sub> windows on 18, 20, 22 May and 13 June. One morning and one afternoon sample were collected on each collection day. Stored samples were frozen below 0°C. Sample analysis was performed at the Advanced Light Source (Lawrence Berkeley National Laboratory, CA) on beamline 5.3.2. Single-particle X-ray absorption spectra were acquired using a combination of scanning transmission X-ray microscopy (STXM) and near-edge X-ray absorption fine structure (NEXAFS) spectroscopy [Russell *et al.*, 2002], which provided relative

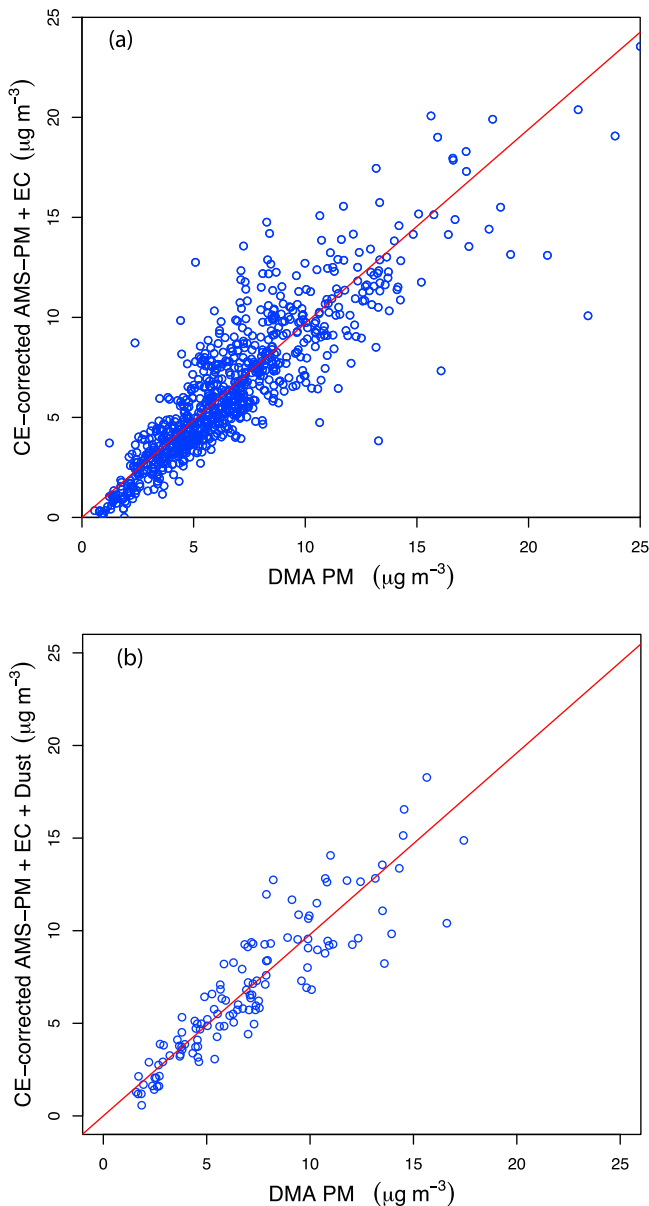


**Figure 1.** (a) Comparison of DMA-measured  $\text{PM}_{500\text{nm}}$  ( $d_m$ ) with the sum of concentrations for AMS-measured  $\text{PM}_{700\text{nm}}$  ( $d_{va}$ ) and EC. Correlation coefficient and slope are 0.88 and 0.97, respectively. Hourly averaged concentrations were used to match the 1 h time resolution of EC measurements. (b) Comparison of DMA-measured  $\text{PM}_{700\text{nm}}$  ( $d_m$ ) with the sum of concentrations for AMS-measured  $\text{PM}_1$  ( $d_{va}$ ), EC, and dusts. Correlation coefficient and slope are 0.90 and 0.98, respectively. Averaged concentrations of 3 h or 6 h (time resolution for FTIR measurements) were used for comparison. Dust was assumed to be a mixture of metal oxides and salts, including  $\text{SiO}_2$ ,  $\text{Al}_2\text{O}_3$ ,  $\text{Fe}_2\text{O}_3$ ,  $\text{Na}_2\text{O}$ ,  $\text{K}_2\text{O}$ ,  $\text{TiO}_2$ ,  $\text{BaO}$ ,  $\text{MnO}$ ,  $\text{CaCO}_3$ , and  $\text{MgCO}_3$  [Usher *et al.*, 2003]; their concentrations were calculated from corresponding elemental concentrations quantified by XRF. In both plots, a CE of 0.8 was used for AMS measurements. The red line in each panel shows the best linear fit for the data points.

quantification of single-particle organic functional groups, including alkane, hydroxyl, ketone, alkene, and carboxylic acid groups. Functional group abundance was quantified using an automated algorithm developed by Takahama *et al.* [2010].

### 2.2.3. Elemental Concentrations

[11] A total of 150  $\text{PM}_1$  and 46  $\text{PM}_{2.5}$  filter samples used for FTIR analysis (65% and 100% of  $\text{PM}_1$  and  $\text{PM}_{2.5}$  samples, respectively) were selectively analyzed using X-ray fluorescence (XRF) at Chester Laboratories (Chester LabNet, Tigard, Oregon). Concentrations of 38 elements (heavier than Ne) were quantified. Elements Al, Si, S, K, Ca, Fe, Co, Zn, and Br were above detection limit in 80% of the samples.

### 2.3. Size-Resolved Organic and Inorganic Mass Fragments for Bulk and Single Particles

[12] A high-resolution time-of-flight aerosol mass spectrometer (HR-ToF-AMS; Aerodyne, Billerica, MA) was deployed to provide high time-resolution measurements of nonrefractory components, including OM, sulfate, nitrate, ammonium, and chloride. Particles passing through a 100  $\mu\text{m}$  pinhole are focused and accelerated by an aerodynamic lens. The accelerated particles impact a heated surface ( $600^\circ\text{C}$ ), and the nonrefractory components flash vaporized and ionized. The ionized vapor fragments are subsequently analyzed by a time-of-flight mass spectrometer [Canagaratna *et al.*, 2007]. The resulting high mass resolution allows the HR-ToF-AMS to separate ions that would otherwise overlap in a relatively low mass resolution quadrupole detector (in a Quadrupole AMS). As a result, the detector provides detailed quantitative elemental compositions from which the O/C, an indicator of the oxidation state of ambient aerosols [Jimenez *et al.*, 2009], can be calculated. The ionization efficiency (IE) of nitrate, which is used to calculate the mass of the fragments, was calibrated using 350 nm  $\text{NH}_4\text{NO}_3$  particles (selected by a scanning differential mobility analyzer) every 3–5 days during the campaign. The relative IE (RIE) of ammonium, derived from the  $\text{NH}_4\text{NO}_3$  calibration, was 4.1 during this study (the default RIE is 4.0 in the standard AMS data analysis software). Particle sizes, measured by the time of flight between a rotating chopper and the vaporizer [Jayne *et al.*, 2000], enable size-resolved chemical composition measurements of submicron particles. A light-scattering (LS) module, coupled with the HR-ToF-AMS, optically detects single particles from a 405 nm laser before particles reach the vaporizer. Light pulses scattered by the particles trigger acquisition of single-particle mass spectra [Cross *et al.*, 2007], enabling real-time measurements of single-particle chemical compositions. The “mass spectrum” (MS) mode (including high S/N “V” mode and high mass resolution “W” mode), the “time-of-flight” (TOF) mode, and the “LS” mode alternated during operation, with approximately a 5 min time resolution for each measurement cycle.

[13] The collection efficiency (CE) of the AMS measurements was evaluated by comparing AMS-measured particle mass to the mass derived from a scanning differential mobility analyzer (DMA; described in section 2.3). Comparisons were made for particles of vacuum aerodynamic diameters ( $d_{va}$ ) smaller than 700 nm and  $d_{va}$  smaller than 1  $\mu\text{m}$  (Figure 1). The 700 nm size cut was selected (in addition to 1  $\mu\text{m}$ ) because smaller particle sizes (60 to 700 nm  $d_{va}$ ) have nearly 100% transmission efficiency [Jayne *et al.*, 2000] and likely compare better with the DMA measurements in the same size range.

AMS-measured  $PM_{700nm}$  and  $PM_1$  were calculated by summing the concentrations of the individual components, each of which was derived by integrating their mass size distributions measured in TOF mode. A factor of 2 was applied to the integrated concentrations (i.e., multiply by 2) to scale the integrated concentration (from the TOF mode measurements) to the concentration measured from the MS-V mode. To account for the missing refractory components, elemental carbon (EC) and the sum of EC and dust were added to  $PM_{700nm}$  and  $PM_1$ , respectively, assuming that dust mainly existed in the larger particles ( $700\text{ nm} - 1\text{ }\mu\text{m}$   $d_{va}$ ). A density ( $\rho$ ) of  $1.4\text{ g cm}^{-3}$  was applied to convert the DMA-measured number concentration to mass concentration, assuming spherical particles [Ahlm *et al.*, 2012]. The density was calculated by converting the vacuum aerodynamic diameter ( $d_{va}$ ) measured by the AMS to the mobility diameter measured by the SMPS ( $d_m$ ), using the equation  $d_m = (d_{va}/\rho) \cdot \rho_0$  [DeCarlo *et al.*, 2004], where  $\rho$  is the effective density and  $\rho_0 = 1.0\text{ g cm}^{-3}$ . Ahlm *et al.* [2012] found that  $\rho = 1.4\text{ g cm}^{-3}$  resulted in the best agreement between the DMA-derived and AMS-measured mass size distributions. Concentrations were calculated by integrating the DMA-derived mass size distributions for particles smaller than 500 nm and 700 nm in mobility diameter ( $d_m$ ), which corresponded to 700 nm and  $1\text{ }\mu\text{m}$  in  $d_{va}$  ( $d_m = d_{va}/\rho$ ), respectively. A set of CE (0.5–1) values was tested, and a CE of 0.80 resulted in the best comparison of the AMS- and DMA-derived masses (slopes are close to 1) for both  $PM_{700nm}$  and  $PM_1$  (Figure 1). Therefore, a CE of 0.8 was assigned to each of the 5 min AMS-measured organic and inorganic components and the PMF factors throughout the campaign.

#### 2.4. Molecular Organic Markers

[14] Speciated organic marker compounds were measured with 1 h or 2 h resolution using thermal desorption aerosol gas chromatograph mass spectrometer (TAG) [Williams *et al.*, 2006; Worton *et al.*, 2011]. The sampling strategy and configuration of TAG in this study are detailed in Y. Zhao *et al.* (Insights into SOA formation mechanisms from measured gas/particle partitioning of specific organic tracer compounds, submitted to *Environmental Science and Technology*, 2012). Briefly, aerosols (gases and particles) passed through a  $PM_{2.5}$  cyclone (SCC BGI Inc., Waltham, MA;  $\sim 5\text{ m}$  above ground level) were collected by a thermal desorption cell. Collected particles are thermally desorbed and transferred into gas chromatograph mass spectrometer for quantification. Gas- and particle-phase organic marker compounds are measured by periodically alternating an active carbon denuder situated downstream of the sampling inlet. The molecular source markers used in this study are from the TAG measurements (particle-phase marker compounds are used) unless otherwise specified.

[15] In addition to in situ measurements using TAG, organic marker compounds were measured from daily filter (prebaked quartz fiber filters) samples that were collected (synchronizing the FTIR  $PM_{2.5}$  sampling time) by high-volume filter samplers (Tisch Environmental Village of Cleves, OH) from 15 May to 30 June 2010. Multiple samplers were operated simultaneously so that multiple sets of samples were collected. One set of the samples was extracted using 125 mL 1:1 (v/v) dichloromethane and methanol mixture for 24 h in a Soxhlet extractor. Filter extracts were

evaporated to dryness, followed by derivatization using 250  $\mu\text{L}$  N,O-bis (trimethylsilyl) trifluoroacetamide (BSTFA) with 1% trimethylchlorosilane (TMCS) and 100  $\mu\text{L}$  pyridine [Jaoui *et al.*, 2004]. The derivatized sample was analyzed by GC-ion trap mass spectrometer (GC-MS; Thermoquest Model GCQ+, Austin, TX), with analysis procedures described previously [Kleindienst *et al.*, 2007, 2012; Offenber *et al.*, 2011]. Another set of samples was spiked with deuterated internal standards (alkanes, polycyclic aromatic hydrocarbons, and cholestane) and extracted using accelerated solvent extraction (Dionex ASE 300) with dichloromethane and methanol (1:1). Extracts were then concentrated to 250  $\mu\text{L}$  and analyzed using an Agilent 7890 GC coupled to an Agilent 5975 MS in electron impact (EI) ionization scan mode [Sheesley *et al.*, 2004]. A third set of the samples was extracted in 15 mL high-purity methanol (LC-MS Chromasolv grade, Sigma-Aldrich) by ultrasonication for 45 min. The extracts were dried under a gentle stream of  $N_2$  gas. Dried extracts were reconstituted using 250  $\mu\text{L}$  1:1 (v/v) solvent mixture of 0.1% acetic acid in water (LC-MS Chromasolv grade, Sigma-Aldrich) and 0.1% acetic acid in methanol (LC-MS Chromasolv grade, Sigma-Aldrich). Reconstituted samples were shaken and sonicated for 5 min before being analyzed by an Agilent ultra performance liquid chromatography (UPLC) system coupled to an Agilent 6520 Series Accurate Mass, high-resolution quadrupole time-of-flight mass spectrometer (Q-TOFMS) equipped with an electrospray ionization (ESI) source operated in the negative ion mode (UPLC/ESI-HR-Q-TOFMS). Detailed operating conditions and spectral analyses are presented in [Zhang *et al.*, 2011].

#### 2.5. Additional Measurements

[16] Other supporting particle-phase and gas-phase measurements included submicron particle number size distributions measured by a custom-built DMA with a time resolution of 11 min [Ahlm *et al.*, 2012], elemental carbon measured using a Sunset real-time EC/OC analyzer (Oregon, USA), ozone monitored by a Dasibi 1008 PC ozone monitor, and OH radicals measured by a ground-based tropospheric hydrogen oxides sensor (GTHOS).

[17] Meteorological measurements included temperature and relative humidity (RH) monitored by a Vaisala HMP45C RH/T sensor, and wind direction and wind speed recorded using an R. M. Young 5103 Wind Monitor.

### 3. Results

[18] OM was the major component in submicron particle mass (56%), followed by dust (12%), sulfate (11%), nitrate (9%), ammonium (8%), and EC (4%) (Figure 2a). In comparison, for particles smaller than 150 nm ( $PM_{150nm}$ ), OM accounted for 76% of the particle mass [Ahlm *et al.*, 2012] (Figure 2c). The submicron OM ( $OM_1$ ) concentration measured by FTIR varied from 0.4 to  $11.5\text{ }\mu\text{g m}^{-3}$ , averaging  $2.4\text{ }\mu\text{g m}^{-3}$  for the entire campaign (Table 1). This OM was substantially lower than the OM measured in Mexico City ( $9.9\text{ }\mu\text{g m}^{-3}$ ) and in the vicinity of Houston ( $4.9\text{ }\mu\text{g m}^{-3}$ ), using the same technique [Liu *et al.*, 2009; Russell *et al.*, 2009]; this suggests lower PM pollution levels at Bakersfield during CalNex than that in Mexico City and Houston. AMS- and FTIR-measured OM closely tracked each other

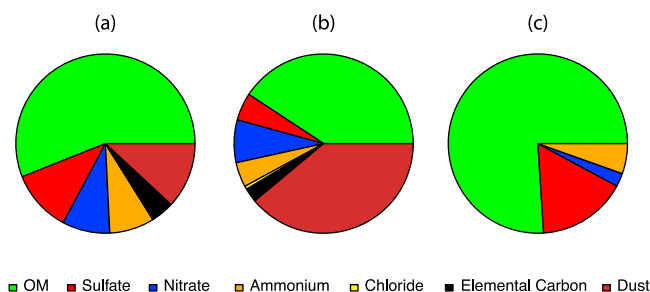


**Figure 2.** Campaign average composition of (a)  $PM_{1}$ , (b)  $PM_{2.5}$ , and (c)  $PM_{150nm}$  [Ahlm *et al.*, 2012]. The OM concentration in  $PM_{1}$  and  $PM_{150nm}$  was measured by the AMS. The OM in  $PM_{2.5}$  was calculated by scaling the AMS-measured  $OM_{1}$  by the FTIR-measured  $OM_{2.5}$ -to- $OM_{1}$  ratio. The concentration of dust in Figures 2a and 2b was calculated using the XRF-measured dust elements in  $PM_{1}$  and  $PM_{2.5}$  as described in Figure 1. EC was not shown in  $PM_{150nm}$  because ultrafine EC measurements were not available.

(Figure 3) with a correlation coefficient ( $r$ ) of 0.77. Linear regression of the two quantities (intercept forced to zero) suggested that the FTIR-measured OM was on average nearly 70% of the CE-corrected AMS-measured OM. Given the measurement uncertainties (25–30% for the FTIR and AMS measurements), the differences lie within the expected range for the two independent measurements. However, the possibility of desorption of semivolatile components from the 3 h or 6 h filter samples could not be ruled out, although the comparability of the AMS-FTIR mass differences for both the 3 h and 6 h samples suggests that volatile losses did not increase with sampling time as is usually expected [Mader *et al.*, 2001].

[19] Major functional groups contributing to  $OM_{1}$  included alkane (35%), hydroxyl (22%), and carboxylic acid (21%) groups, among which carboxylic acid and alkane groups correlated with an  $r$  of 0.90. Similar correlation between these two groups was observed previously [Liu *et al.*, 2011], suggesting that carboxylic acid and alkane groups formed from the same source and likely via the same mechanism, likely by photooxidation of gas-phase alkane molecules [Russell *et al.*, 2011]. Nonacid carbonyl groups, typically associated with oxidation products of aromatic compounds [Lee and Lane, 2010], accounted for 11% of the OM. Amine groups (9% OM) were likely associated with bovine

**Table 1.** Campaign Average OM Measured by FTIR and AMS and Organic Functional Group Concentrations Measured by FTIR ( $\mu\text{g m}^{-3}$ ) in  $PM_{1}$  and  $PM_{2.5}$ <sup>a</sup>

	FTIR $_{PM1}$	FTIR $_{PM2.5}$	AMS
OM	2.42 ± 1.68	3.24 ± 1.42	4.23 ± 2.75
Alkane	0.85 ± 0.73 (35%)	1.09 ± 0.45 (34%)	-
Hydroxyl	0.53 ± 0.58 (22%)	0.98 ± 1.00 (30%)	-
Carboxylic acid	0.51 ± 0.58 (21%)	0.61 ± 0.29 (19%)	-
Nonacid carbonyl	0.26 ± 0.24 (11%)	0.14 ± 0.20 (4%)	-
Amine	0.22 ± 0.18 (9%)	0.33 ± 0.15 (10%)	-
Organonitrate	0.05 ± 0.05 (2%)	0.07 ± 0.06 (2%)	-
Organosulfate	BDL	0.02 ± 0.04 (1%)	-

<sup>a</sup>Functional group mass fractions are shown in parentheses.

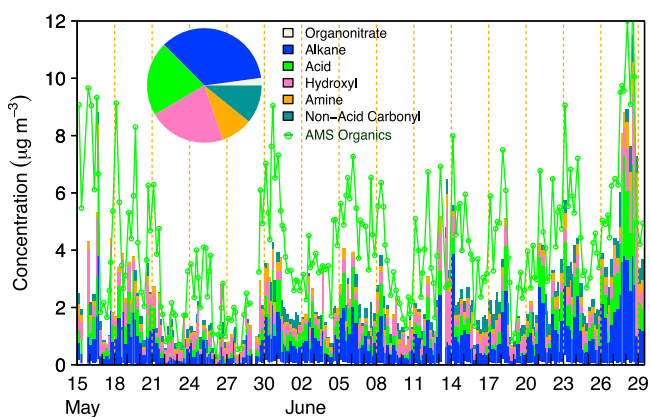


**Figure 3.** Time series of FTIR-measured organic functional group concentrations (stacked bars) in  $PM_{1}$  and AMS-measured OM (green line). The pie chart shows campaign average functional group composition in  $PM_{1}$ .

emissions in the region, as animal husbandry operations are major sources of atmospheric ammonia and amines [Schade and Crutzen, 1995]. Organosulfate groups were below detection limit for all submicron particles and identified as 1% of  $OM_{2.5}$  (Table 1), which is consistent with the low mass of organosulfate molecules ( $\sim 0.2\%$  OM) measured by UPLC/ESI-HR-Q-TOFMS at the same site.

[20] To identify particle types, normalized FTIR ( $PM_{1}$ ) spectra were grouped using the hierarchical clustering technique with the Ward algorithm [Liu *et al.*, 2009; Russell *et al.*, 2009; Ward, 1963]. In the Ward algorithm, each IR spectrum is initially considered as one category. The spectra are progressively merged by minimizing the sum-of-square errors. By selecting a level of branching ( $k$ ), the spectra can be grouped into  $k$  clusters. Using  $k \geq 5$  resulted in at least two clusters that had similar functional group compositions, indicating splitting of certain clusters into smaller clusters that are not distinguishable. Hence  $k = 4$  was selected as the largest number of clusters without splitting, resulting in four chemically distinct clusters (Figure 4). Particles in Cluster 1 had the largest fraction of nonacid carbonyl groups (15%) among the four clusters, with alkane, hydroxyl, and carboxylic acid groups contributing 29%, 28%, and 16% to the OM, respectively. Cluster 2 particles were mainly composed of alkane (42%) and carboxylic acid (29%) groups. Together, Cluster 1 and Cluster 2 accounted for 93% of the submicron FTIR spectra. Spectra in Cluster 3 were characterized by sharp alkane group peaks and had the largest fraction of alkane groups (52%) among the four clusters. Cluster 4 represented particles that were mainly composed of hydroxyl groups (65%). The distinct chemical composition of the four clusters indicated differing contributions from various sources and processes throughout the study.

[21] We found  $m/z$  44 ( $\text{CO}_2^+$ ) accounted for 10% of AMS-measured OM. AMS-measured sulfate, nitrate, and ammonium contributed almost equally to  $PM_{1}$ , the mass fraction ranging from 8% to 11% on average. Using these three components in an ion balance calculation revealed that the  $PM_{1}$  positive ions (ammonium) were 20% higher than that of the negative ions ( $2 \times \text{sulfate} + \text{nitrate}$ ). The time series of the positive and negative ions correlated with an  $r$  of 0.99, indicating that these ions likely formed and condensed simultaneously, i.e., sulfuric

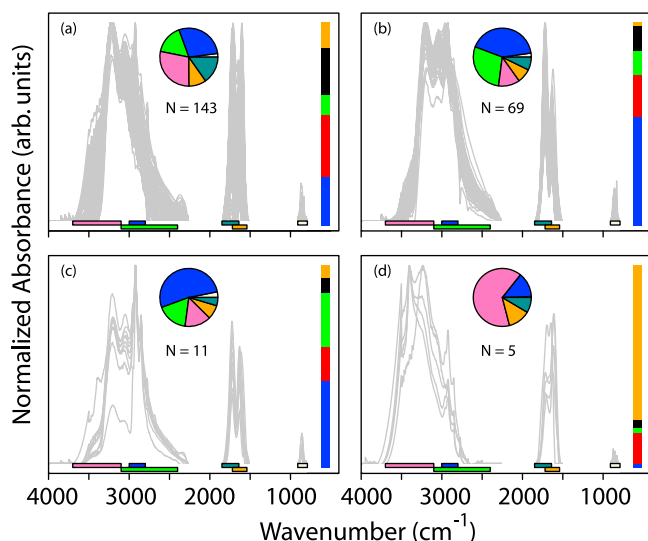


**Figure 4.** FTIR spectra during CalNex for (a) cluster 1 (143 spectra), (b) cluster 2 (69 spectra), (c) cluster 3 (11 spectra), and (d) cluster 4 (5 spectra). Horizontal bars represent functional group absorbance ranges: hydroxyl (pink), carboxylic acid (green), alkane (blue), nonacid carbonyl (teal), amine (orange), and organonitrate (beige). Pie chart shows the average functional group composition in each cluster. Vertical bar represents the average relative contributions of the FTIR factors in each clusters, with colors indicating alkane SOA (blue), aromatic SOA (red), nighttime OA (green), PO SOA (black), and vegetative detritus (orange).

acid and nitric acid interact with ammonia to form ammonium sulfate and ammonium nitrate salts, respectively, followed by condensation of the salts into preexisting particles. High ammonium levels in Bakersfield aerosols are consistent with large ammonia emissions in the SJV [Sorooshian *et al.*, 2008]. The excess ammonium (relative to inorganic sulfate and nitrate) was likely formed by reaction of ammonia with secondary organic acids, such as phthalic acid [Na *et al.*, 2007; Zhao *et al.*, submitted manuscript, 2012]. Because the excess ammonium (relative to inorganic sulfate and nitrate) was  $\sim 50\%$  less (in molar concentration) than the FTIR-measured carboxylic acid groups, the aerosol might be slightly acidic.

[22] Elemental ratios (H/C and O/C) measured by the HR-ToF-AMS are illustrated in the Van Krevelen diagram space (Figure 5). The Van Krevelen diagram, displayed as H/C versus O/C, has proven to be useful for describing evolution of atmospheric organic aerosols [Heald *et al.*, 2010; Ng *et al.*, 2011]. For example, conversion of alkane groups ( $-\text{CH}_2-$ ) to carbonyl groups ( $-\text{C}(=\text{O})-$ ) results in a slope of  $-2$  (addition of 1 oxygen and loss of 2 hydrogen atoms), whereas processes that convert alkane groups to hydroxyl groups ( $-\text{OH}$ ) have a slope of 0. Consequently, formation of hydroxycarbonyl or carboxylic acid groups yields a slope of  $-1$ . The O/C and H/C in this study ranged from 0.02 to 0.62 and from 1.28 to 1.99, respectively. The points in the Van Krevelen diagram can be grouped into two categories that have different slopes. The relatively high-temperature points have a slope of  $-0.93$ , while the slope of the low-temperature points is  $-1.3$  (Figure 5). The distinct slope and temperature

for the two categories suggest different chemical and physical processes, including oxidation, condensation, volatilization, and mixing, between daytime and nighttime hours. The measured O/C and H/C in both categories were strongly anticorrelated ( $r = -0.94$  to  $-0.92$ ), suggesting these atmospheric processes changed the O/C and H/C along straight lines. The slopes of  $-0.93$  and  $-1.3$  of the linear fit from this study was similar to the slope of  $-1.1$  observed during the SOAR-1 (Study of Organic Aerosol at Riverside) measurements at Riverside [Heald *et al.*, 2010], but organic aerosol composition at Bakersfield had larger ranges of O/C and H/C than at Riverside (O/C and H/C varied in 0.2–0.5 and 1.4–1.7, respectively, during SOAR-1), which reflects the larger variety of emission sources at Bakersfield.

[23] Compared to  $\text{PM}_{10}$ ,  $\text{PM}_{2.5}$  was composed of a larger fraction of dust components (39%) and a lower fraction of OM (41%) (Figure 2b). Dust components were mainly composed of elements Ca, Si, Al, and Fe (more likely by their oxides and salts). OM in  $\text{PM}_{2.5}$  ( $\text{OM}_{2.5}$ ) was largely (75%) in submicron particles. The mass difference between  $\text{OM}_1$  and  $\text{OM}_{2.5}$  (55% of  $\text{OM}_1$ ) can be explained by the hydroxyl groups, suggesting that they were associated with larger particles such as dust components (details in following section). Scaling the AMS-measured  $\text{OM}_1$  by the  $\text{OM}_{2.5}$ -to- $\text{OM}_1$  ratio measured by FTIR, the calculated AMS  $\text{OM}_{2.5}$  was  $5.6 \mu\text{g m}^{-3}$ , which is comparable to the  $\text{OM}_{2.5}$  ( $\sim 6\text{--}7 \mu\text{g m}^{-3}$ ) measured during May–June 1999–2001 at Bakersfield [Chow *et al.*, 2006a].

### 3.1. Identification of Organic Mass Sources

[24] The main factors contributing to the OM were identified separately from FTIR ( $\text{PM}_{10}$  and  $\text{PM}_{2.5}$ ) and AMS measurements using positive matrix factorization (PMF) method (PMF2) [Paatero and Tapper, 1994]. PMF procedures are described in the appendices. The factors were identified primarily by their correlations with particle-phase source

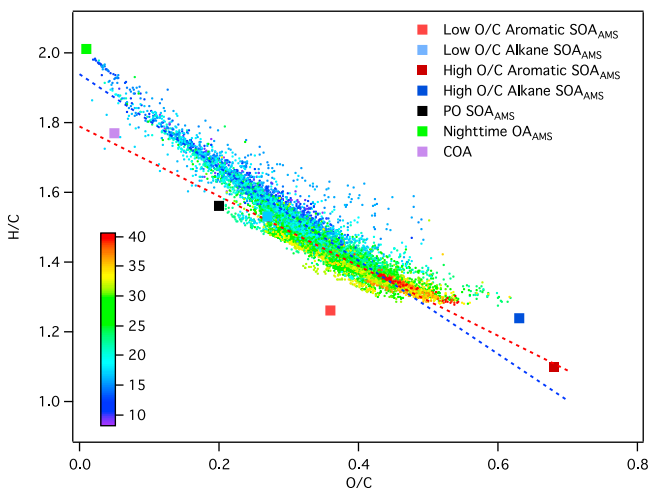


**Figure 5.** Van Krevelen diagram (H/C versus O/C) from the AMS measurements. The points are colored by temperature ( $^{\circ}\text{C}$ ), with the scale shown by the vertical bar. The points with temperature greater and less than  $25^{\circ}\text{C}$  are fitted by the red and blue dashed lines, respectively. The slopes of the red and blue lines are  $-0.93$  and  $-1.3$ , respectively. The intercepts of the red and blue lines are 1.76 and 1.91, respectively.

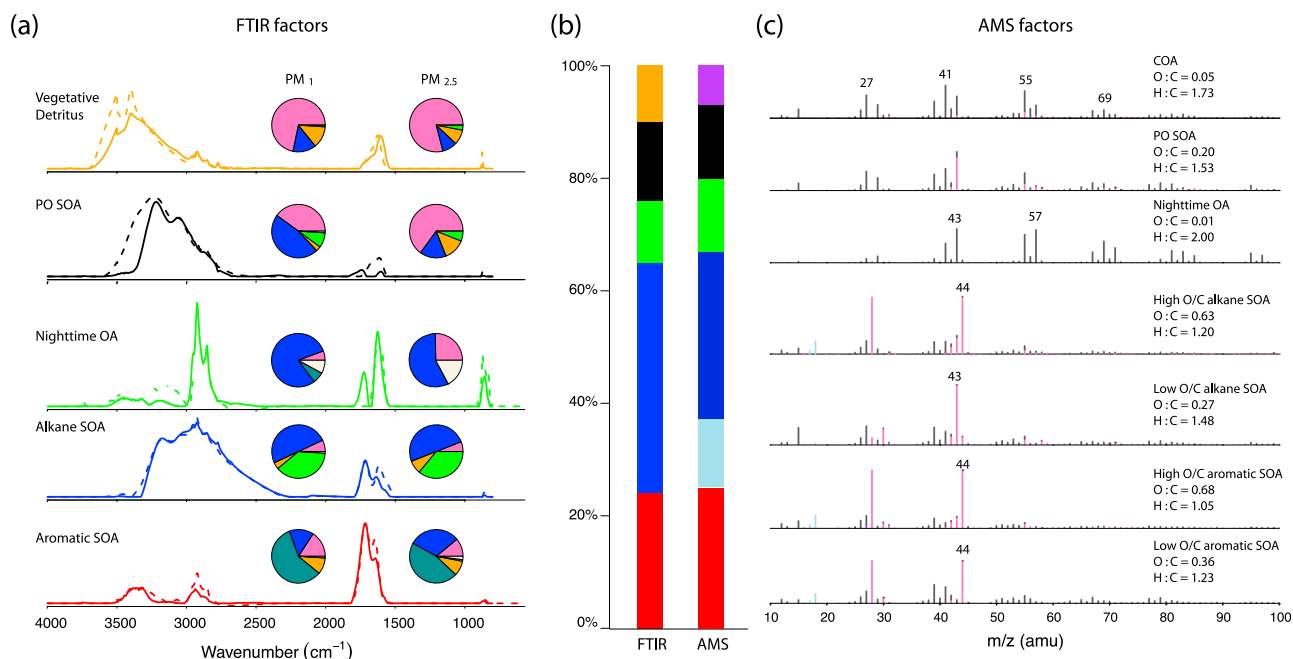


**Figure 6.** (a) FTIR factor spectra derived from PM<sub>1</sub> (solid line) and PM<sub>2.5</sub> (dashed line) measurements. The pie charts show factor compositions, with functional groups as follows: alkane (blue), hydroxyl (hot pink), carboxylic acid (green), nonacid carbonyl (teal), and organonitrate (beige) functional groups. (b) Campaign average mass fractions of FTIR PM<sub>1</sub> and AMS factors. Colors indicate aromatic SOA (red) (red and dark red for the AMS low and high O/C aromatic SOA factors, respectively), alkane SOA (blue) (light blue and dark blue for the AMS low and high O/C alkane SOA factors, respectively), nighttime OA (green), PO SOA (black), and vegetative detritus (orange), and COA (purple) factors. (c) Normalized mass spectra of AMS factors.

markers, facilitated by comparisons of factor composition and spectra to factors identified from past studies. Pearson's correlation coefficients ( $r$ ) are used in this study. The correlations were done at the highest time resolution possible with the tracer measurements. The time resolution of the AMS, TAG, and XRF measurements was  $\sim 5$  min, 1–2 h, and 3–6 h, respectively. Subscripts “FTIR,” “FTIR2.5,” and “AMS” denote the factors commonly identified from FTIR PM<sub>1</sub>, FTIR PM<sub>2.5</sub>, and AMS measurements. Detailed factor identification procedures are presented below.

### 3.1.1. Factors Identified From FTIR PM<sub>1</sub> and PM<sub>2.5</sub> Measurements

[25] Five factors were identified from each of the FTIR PM<sub>1</sub> and PM<sub>2.5</sub> measurements (auxiliary material).<sup>1</sup> The PM<sub>1</sub> and PM<sub>2.5</sub> factors were similar in factor spectra and compositions (Figure 6a), indicating nearly the same factors were found for OM<sub>1</sub> and OM<sub>2.5</sub>, which is consistent with the fact that 75% of OM<sub>2.5</sub> was in OM<sub>1</sub>.

[26] The first factor covaried in time with polycyclic aromatic hydrocarbon (PAH) oxidation products 2 H-1-benzopyran-2-one, dibenzofuran, 1,8-naphthalic acid/anhydride, benzophenone, 4-hydroxy-9-fluorenone, and phthalic acid/anhydride [Kautzman *et al.*, 2010; Lee and Lane, 2009, 2010; Webb *et al.*, 2006] measured by TAG (Table S1a in auxiliary material Text S1) and phthalic acid ( $r = 0.7$ )

measured by GC-MS. The factor composition, largely composed of nonacid carbonyl groups (59%), was consistent with oxidation products for aromatic hydrocarbons [Chan *et al.*, 2009; Jaoui *et al.*, 2008; Russell *et al.*, 2011], including PAH and light aromatic compounds. Therefore, this factor was identified as an aromatic SOA factor, representing SOA formed from aromatic hydrocarbons (PAHs and light aromatic compounds) that were likely emitted from gasoline- and diesel-powered vehicles [Schauer *et al.*, 1999, 2002b]. This factor had the greatest contribution (31%) to Cluster 1 particles (Figure 4).

[27] The time series of the second factor correlated most strongly to the time series of C<sub>11</sub>–C<sub>14</sub> ketones (undecanone, dodecanone, tridecanone, and tetradecanone) with  $r$  of 0.63 to 0.77 for the PM<sub>1</sub> factor and 0.58 to 0.90 for the PM<sub>2.5</sub> factor (Tables S1a and S1b in auxiliary material Text S1). Note that the enhanced correlations for the PM<sub>2.5</sub> factor were likely caused by the longer duration of these daily samples, which averaged out any offsets between the time of formation in the gas and particle phases. The long-chain (C<sub>11</sub>–C<sub>14</sub>) ketones are suggested to be first-generation alkane oxidation products [Lim and Ziemann, 2005, 2009], indicating that this component likely formed from alkane oxidation processes. The factor spectra and functional group compositions were nearly identical to the fossil fuel combustion factors identified from the shipboard measurements near Houston and the ground-based measurements in Southern California, which were suggested to originate from alkane oxidation processes

<sup>1</sup>Auxiliary materials are available in the HTML. doi:10.1029/2012JD018170.

**Table 2.** Summary of O/C Values for Primary or HOA Components From Previous Studies and O/C of SOA Components in This Study

Source Type	O/C <sup>a</sup>	References
Primary OA	<0.1	This study
HOA (New York City)	0.06	<i>Sun et al.</i> [2011]
HOA (Mexico City aircraft)	0.06	<i>DeCarlo et al.</i> [2004]
Diesel exhaust	0.03, 0.05	<i>Aiken et al.</i> [2008], <i>Nakao et al.</i> [2011]
Gasoline exhaust	0.04	<i>Aiken et al.</i> [2008]
Cooking emission	0.08–0.13	<i>He et al.</i> [2010]
COA	0.11	<i>Huang et al.</i> [2010]
COA	0.05	This study
Nighttime OA	0.01	This study
Secondary OA	0.20–0.68	This study
Alkane SOA	0.27–0.63	This study
Aromatic SOA	0.36–0.68	This study
PO SOA	0.20	This study

<sup>a</sup>AMS-measured O/C excludes organonitrate and organosulfate contributions to O as the nitrate and sulfate components were not distinguishable from inorganic.

[*Hawkins and Russell*, 2010; *Liu et al.*, 2011; *Russell et al.*, 2009]. Thus this factor was denoted as the alkane SOA factor.

[28] The third factor from the PM<sub>1</sub> factor analysis correlated ( $r$  of 0.65) to pinonaldehyde measured by TAG and 3-Hydroxyglutaric acid ( $r$  of 0.5) measured by GC-MS, which are markers for biogenic SOA formed from oxidation of  $\alpha$ -pinene [*Hallquist et al.*, 1999; *Claeys et al.*, 2007]. This factor, observed in high concentrations at night, was largely composed of alkane groups (79%) and had the largest mass fraction (8%) of organonitrate groups of all the factors; its composition was consistent with products from  $\alpha$ -pinene and  $\beta$ -pinene oxidation by NO<sub>3</sub> radicals [*Hallquist et al.*, 1999; *Wängberg et al.*, 1997]. However, the factor showed a weaker correlation ( $r \leq 0.50$ ) to PAH compounds, suggesting a contribution of primary anthropogenic sources to this factor. Thus, this factor was determined to be the nighttime biogenic SOA factor mixed with less oxygenated hydrocarbon-like anthropogenic emissions and denoted as nighttime OA. The PM<sub>2.5</sub> nighttime OA factor had similar composition to the PM<sub>1</sub> nighttime OA factor, being dominated by alkane (57%) and organonitrate (17%) groups, but also contained a larger hydroxyl group mass and enhanced correlations to dust elements. Thus, the PM<sub>2.5</sub> nighttime OA factor likely included a small fraction of dust-related organic components.

[29] The fourth factor of PM<sub>1</sub> correlated ( $r$  of 0.6) to the crude oil marker V (vanadium) [*Khalaf et al.*, 1982]. Its IR spectrum was comparable to the “oil combustion/refining” factor spectrum identified from the shipboard measurements near Houston [*Russell et al.*, 2009]. The high mass fraction (40% to 65%) of hydroxyl groups indicates that this factor was likely formed as secondary products in the atmosphere. The factor was identified as a petroleum operation SOA (PO SOA) factor, representing the oil extraction and refinery operations north and northwest of Bakersfield. The most commonly used method for oil extraction in this area, steam injection, heats crude oil using high-temperature steams. The heated crude oil has reduced viscosity and therefore is easier to pump [*Fatiemi and Jamaloei*, 2011]. The high-temperature steam comes from steam generators, which usually burn crude oil and likely emits V-rich pollutants in addition to NO<sub>x</sub>, CO,

and hydrocarbons [*Myers*, 1986]. The corresponding PM<sub>2.5</sub> factor spectrum was comparable to that of the PM<sub>1</sub> factor (Figure 6a), suggesting that they are the same factors. It is worth noting that V in PM<sub>2.5</sub> correlated well with dust elements, such as V correlating to Si with an  $r$  of 0.96 in PM<sub>2.5</sub> that is much greater than the correlation of V and Si ( $r = 0.35$ ) in PM<sub>1</sub>, indicating that V in PM<sub>2.5</sub> was largely from dust sources [*Chow et al.*, 2003], resulting in a weakly negative correlation of the PO SOA factor and V in PM<sub>2.5</sub>. The average concentration of the PO SOA factor peaked in the afternoon, which was consistent with the daytime northwesterly winds from the direction of the oil drilling and the associated petroleum operation activities located to the northwest of the sampling site.

[30] The fifth factor of the PM<sub>1</sub> and PM<sub>2.5</sub> solutions correlated to the dust elements Si, Al, Ca, and Mg, suggesting that this factor represented organic components associated with dust particles. Double peaks at 2850 cm<sup>-1</sup> and 2920 cm<sup>-1</sup>, along with a strong spectral absorption at 3500 cm<sup>-1</sup>, indicated the existence of repeating methylene and phenol groups, which likely originated from plant wax [*Hawkins and Russell*, 2010] and plant lignin compounds [*Cass*, 1998], respectively. The large fraction of hydroxyl groups (71% to 79%) in this factor was consistent with saccharide-type compounds in plant materials [*Bianchi et al.*, 1993]. Association of the factor with dust and plant components suggests that this factor was likely from vegetative detritus that resuspended with dust particles. This factor was denoted as a vegetative detritus factor and appeared predominantly in Cluster 4 particles (Figure 4).

### 3.1.2. Factors Identified From AMS Measurements

[31] Six or seven factors were identified from the AMS measurements. The factors in the 6- and 7-factor solutions had similar factor time series and mass spectra (auxiliary material Figures S7 and S8). Compared to the 6-factor solution, an additional factor with high O/C (named as high O/C alkane SOA and discussed below) was identified in the 7-factor solution. We present both the 6- and 7-factor solutions to show the consistency and variability of the PMF factors. The factor  $m/z$  spectra, O/C, and H/C are shown in Figure 6c and auxiliary material Figure S7.

[32] The first factor correlated strongly ( $r$  of 0.81 to 0.90) to particle-phase PAH marker compounds (Table S2a in auxiliary material Text S1), which are usually coemitted with light aromatic compounds in vehicular exhausts. This factor was characterized by a strong peak at  $m/z$  44 and had an O/C of 0.36, which was higher than the typical O/C of HOA components ( $\sim 0.10$ ) observed in laboratory and field studies (Table 2) but in the O/C range of 0.20 to 0.60 for SV-OOA (semivolatile OOA) identified from a number of AMS measurements [*Ng et al.*, 2010]. Thus, it suggests that this factor was oxidized but associated with a low oxidation state and, so, was termed low O/C aromatic SOA factor.

[33] Compared to the low O/C aromatic SOA factor, the second factor more closely correlated to long-chain alkanes and alkane SOA components (Tables S2a and S2b in auxiliary material Test S1), suggesting that this factor likely originated from alkane-related sources. The H/C of this factor was 21% higher than the O/C of the low O/C aromatic SOA factor (Figure 6c). This result is consistent with the expectation of a higher H/C for alkane SOA than aromatic SOA: Since alkanes are more saturated than aromatics,

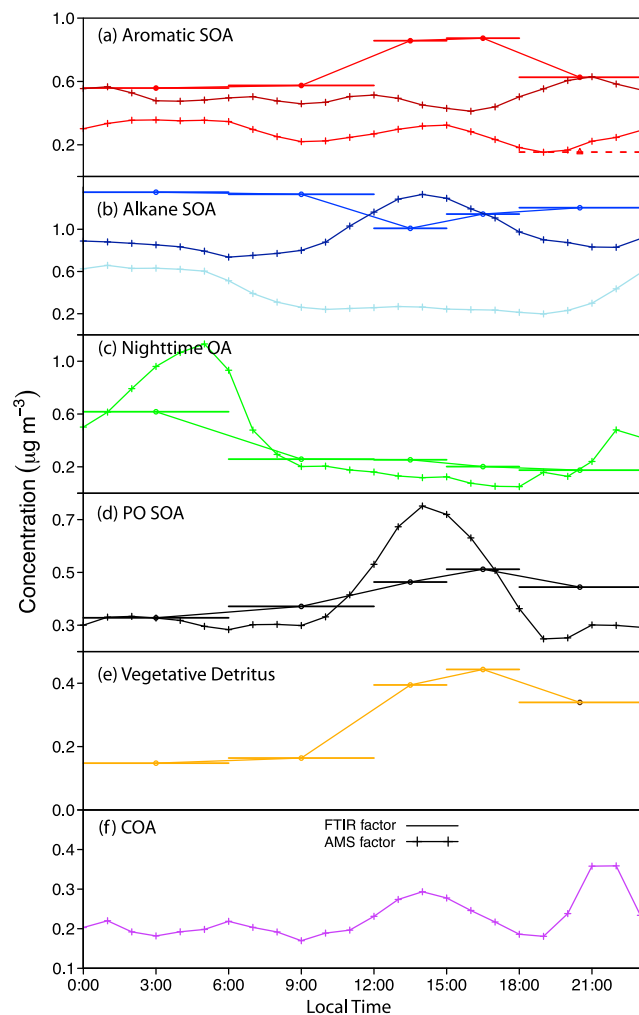


**Figure 7.** Diurnal cycles for (a) aromatic SOA<sub>FTIR</sub> (red), low O/C aromatic SOA<sub>AMS</sub> (red), and high O/C aromatic SOA<sub>AMS</sub> (dark red), (b) alkane SOA<sub>FTIR</sub> (blue), low O/C alkane SOA<sub>AMS</sub> (light blue), and high O/C alkane SOA<sub>AMS</sub> (dark blue), (c) nighttime OA<sub>FTIR</sub> (green) and nighttime OA<sub>AMS</sub> (green), (d) PO SOA<sub>FTIR</sub> (black) and PO SOA<sub>AMS</sub> (black), (e) vegetative detritus (orange), and (f) COA (purple) factors. In each panel, horizontal bars represent FTIR factors (PM<sub>1</sub> samples), with bar lengths indicating sampling duration; lines with markers represent AMS factors.

alkane SOA is expected to be less oxygenated than aromatic SOA. As the factor O/C (0.27) was higher than expected for primary OM ( $\sim 0.10$ ) (Table 2), it was identified as a low O/C alkane SOA factor.

[34] The third factor had the highest O/C (0.68–0.72) of all the factors, suggesting that this factor is also secondary but more oxidized than the first two factors—possibly because they formed in later generations [Jimenez *et al.*, 2009]. The factor spectrum was nearly identical and resembled those of LV-OOA (low-volatility OOA) [Ulbrich *et al.*, 2009]. The time series of this factor correlated most strongly to PAH SOA marker compounds, suggesting that this factor likely represented the oxidation products of aromatic hydrocarbons, including light aromatics and PAH. This factor was

identified as a high O/C aromatic SOA factor. The high O/C aromatic SOA factors in the 6- and 7-factor solutions had similar time series, with the former associated with greater mass concentration (auxiliary material Figures S7 and S8).

[35] The fourth factor, the additional factor identified in the 7-factor solution, had similar mass spectra to the high O/C aromatic SOA factor. This factor correlated to both PAH SOA and alkane SOA markers. While the similarity of the factor spectra and correlations with source markers make it difficult to distinguish this factor and the high O/C aromatic SOA factor, their diurnal cycles were different (Figures 7a and 7b). The high O/C aromatic SOA factor peaked at noon and in the evening (2000 h), while the fourth factor had a broad peak centered at 1500 h. Distinct diurnal cycles suggested different formation pathways. The high O/C aromatic SOA factor and the fourth factor correlated weakly to long-chain alkane compounds (e.g., heptadecane and octadecane in Table S2b in auxiliary material Text S1), with the latter having stronger correlations ( $r$  of 0.25 to 0.27 for the high O/C aromatic SOA factor and  $r$  of 0.37 to 0.38 for the fourth factor). Furthermore, enhanced correlations to alkane compounds of 0.63 to 0.72 resulted from daily averaged concentration of the fourth factor, but such a large enhancement was not observed under the same conditions for the high O/C aromatic SOA factor ( $r$  of 0.37 to 0.46). This suggests that the fourth factor was likely largely linked to alkane-related sources, although contribution of aromatic SOA to this factor cannot be entirely ruled out. Accordingly, the fourth factor was defined as a high O/C alkane SOA factor. The higher H/C ratio of the high O/C alkane SOA compared to the high O/C aromatic SOA is consistent with the expectation that alkane SOA contains more C-H bonds than aromatic SOA, given that the precursor alkanes are more saturated than aromatics. The high O/C alkane SOA factor accounted for 71% of total alkane SOA, which includes high and low O/C alkane SOA components. This mass fraction is consistent with mechanism simulation that suggests more than 67% of alkane SOA was fourth-generation and higher products after 10 h of reactions [Yee *et al.*, 2012].

[36] Concentrations of the fifth factor peaked at night (Figure 7c), having been associated with nighttime easterly and southeasterly winds. This pattern compares to that of monoterpenes and their oxidation products (e.g., pinoaldehyde), which suggests contributions from biogenic sources to this factor. The very low O/C ( $< 0.1$ ) also indicates a contribution from primary OM. The mass spectrum was similar to the spectrum of HOA (hydrocarbon-like organic aerosol) [Ulbrich *et al.*, 2009] (see also <http://cires.colorado.edu/jimenez-group/AMSsd>), indicating unoxidized primary anthropogenic sources. As such, this factor was identified as nighttime OA.

[37] The sixth factor had a stronger correlation with V than any other source markers. In addition, the factor's diurnal cycle matched the diurnal cycle of V, suggesting organic components from petroleum operations. The factor was characterized by  $m/z$  43 (87% C<sub>2</sub>H<sub>3</sub>O<sup>+</sup> and 13% C<sub>3</sub>H<sub>7</sub><sup>+</sup>) with an O/C of 0.20, which is larger than 0.10 that is typical for HOA (Table 2). For this reason, this factor is considered secondary rather than primary and termed petroleum operation SOA (PO SOA).

[38] The seventh factor was identified as a cooking organic aerosol (COA) factor for two reasons: The factor

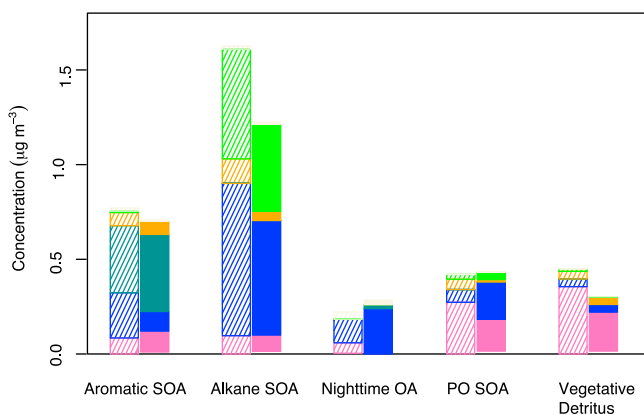


**Figure 8.** Mass concentration comparison of FTIR  $PM_1$  and  $PM_{2.5}$  factors. Striped and solid bars indicate  $PM_1$  and  $PM_{2.5}$  factors, respectively. Color assignments for functional groups are the same as in Figure 3.

spectrum was similar to previously identified COA factor mass spectra [Huang *et al.*, 2010; Mohr *et al.*, 2012] that were characterized by  $m/z$  27, 41, 55, and 69 with  $\Delta m/z$  of 14, fragments specific for unsaturated fatty acids emitted from cooking activities [He *et al.*, 2010]; and the factor correlated to the food cooking marker hexadecanoic acid (Tables S2a and S2b in auxiliary material Test S1) [Allan *et al.*, 2010; He *et al.*, 2004]. Further, a low O/C (0.05) suggests that this factor was simply recondensed cooking oils from local sources that had undergone little or no oxidation in the atmosphere.

[39] We have focused on the 7-factor solution in the following discussions since it may suggest differences in the oxidation products formed with time.

### 3.1.3. Comparison of FTIR ( $PM_1$ and $PM_{2.5}$ ) and AMS Factors

[40] The FTIR  $PM_1$  and  $PM_{2.5}$  factors were similar in compositions but differed in mass. Overall, the reconstructed ratio of  $OM_1$  (the sum of  $PM_1$  factors) to  $OM_{2.5}$  (the sum of  $PM_{2.5}$  factors) was 0.85, 13% higher than the actual measured  $OM_1/OM_{2.5}$  of 0.75. The greatest difference between  $PM_1$  and  $PM_{2.5}$  factors was observed in the vegetative detritus factor, the OM being 55% higher in  $PM_{2.5}$ . This difference was largely (92%) attributed to hydroxyl groups (Figure 8), which likely originated from plant materials and then mixed with dusts to result in a larger fraction with bigger particles. The aromatic SOA and alkane SOA factors were 12% and 33% higher, respectively, in  $PM_{2.5}$ , with the alkane groups accounting for the largest difference in each pair of factors. As aforementioned, the nighttime  $OA_{FTIR2.5}$  likely had some dust fractions, indicating incomplete separation of this factor from  $PM_{2.5}$  samples, so nighttime  $OA_{FTIR2.5}$  was slightly smaller than nighttime  $OA_{FTIR}$ . The  $PO_{SOA_{FTIR}}$  was higher in the alkane group mass and lower in the hydroxyl group mass compared to the  $PO_{SOA_{FTIR2.5}}$ , resulting in comparable total OM between the two factors.

[41] The factors identified from AMS measurements show consistencies and differences to the factors derived from FTIR measurements. The low O/C and high O/C aromatic  $SOA_{AMS}$  factors, taken together, correlated to aromatic  $SOA_{FTIR}$  with an  $r$  of 0.73 (auxiliary material Figure S9).

The sum of the low and high O/C aromatic  $SOA_{AMS}$  factors accounted for 25% of OM, consistent with the OM fraction (24%) of the aromatic  $SOA_{FTIR}$  factor (Figure 6b). Similarly, good correlation ( $r = 0.74$ ) was observed for the sum of the low and high O/C alkane  $SOA_{AMS}$  factors and the alkane  $SOA_{FTIR}$  factor, each of which accounted for 41% to 42% of the OM. The difference between the FTIR and AMS high O/C factors can be seen from Figure 7: The diurnal cycle of the alkane  $SOA_{FTIR}$  is more similar to the low O/C alkane  $SOA_{AMS}$  than the total alkane  $SOA_{AMS}$ , and the diurnal cycle of the aromatic  $SOA_{FTIR}$  is more similar to the high O/C aromatic  $SOA_{AMS}$  than the total aromatic  $SOA_{AMS}$ . The difference in diurnal cycles may result from the scatter in their correlations as well as the uncertainties of the measurements and factorization. The  $PO_{SOA_{AMS}}$  and  $PO_{SOA_{FTIR}}$  (correlated with an  $r$  of 0.52) contributed 13% to 14% of OM. The campaign average mass fractions of  $NOA_{FTIR}$  and  $NOA_{AMS}$  factors were 10% to 13%, with higher fractions of 21% to 24% during 0000–0600 h. The difference between  $NOA_{FTIR}$  and  $NOA_{AMS}$  is that  $NOA_{FTIR}$  includes a substantial contribution of organonitrate functional groups (and a higher associated O/C from them) whereas the organonitrate mass was not distinguishable from the inorganic nitrate in the AMS. However, the AMS measurements were likely more sensitive to smaller particles that may have included a larger fraction of HOA that was not resolved by the FTIR PMF. These differences likely resulted in the relatively low correlation ( $r = 0.52$ ) between  $NOA_{FTIR}$  and  $NOA_{AMS}$ . The vegetative detritus factor (10% OM) was identified only from FTIR measurements, likely because this component was mixed with dust in particles of 500 nm and larger, which have reduced transmission efficiency in the AMS aerodynamic lens and could not be detected effectively by the AMS. The  $COA_{AMS}$  (7% OM) was not found in the FTIR measurements. This difference between the AMS and FTIR factors may be due to COA components mainly existing as small particles (100–200 nm, as discussed in section 4.3), where the small-particle collection efficiency of 1  $\mu m$  Teflon filters drops off [Liu and Lee, 1976] and the small mass in this size range were insufficient for detection.

[42] In summary, factors identified from  $PM_1$  and  $PM_{2.5}$  FTIR and AMS measurements showed good agreement in source type, mass fraction, and time series. The missing vegetative detritus factor for the AMS measurements and COA factor for the FTIR measurements contributed 10% of OM in  $PM_1$ , and both were within the expected uncertainties for each technique. The high O/C aromatic and alkane SOA factors were mathematically independent ( $r < 0.7$ ) but their mass spectra were chemically similar (cosine similarity was 0.99) (cosine similarity is defined as cosine of the angle between two vectors [Stein and Scott, 1994], values ranging from 0 to 1, with higher values indicating higher similarity), thus source markers are needed to justify separation of these factors; in contrast, the FTIR aromatic and alkane SOA factors were mathematically independent ( $r < 0.5$ ) and their IR spectra were chemically different (e.g., cosine similarity was 0.3), thus source markers are not needed to justify separation of the FTIR factors but provide a link to their precursors. The FTIR and AMS factors suggested that 80% to 90% of OM was secondary, even those measurements conducted near emission sources. Of these SOA components,

**Table 3.** Source Inventory of PM<sub>2.5</sub> for Kern County in the San Joaquin Valley in 2008 (<http://www.arb.ca.gov/ei/emissiondata.htm>) Shown as Percentage of PM<sub>2.5</sub> and Sources Identified in This Study Shown as Percentage of OM<sub>2.5</sub>

Source Type	Inventory (%)	This Study (%)
Mobile motor sources	31 (80) <sup>a</sup>	65
Petroleum production and refining	0 (1)	14
Miscellaneous processes		
Dust	16 (14)	10
Cooking	2 (4)	7
Residential fuel combustion	7	ND <sup>b</sup>
Farming operations	9	ND
Construction and demolition	1	ND
Managed burning and disposal	6	ND
Fuel (mainly natural gas) combustion	14	ND
Industrial processes	13	ND
Solvent evaporation	0	ND
Waste disposal	0	ND
Cleaning and surface coatings	0	ND

<sup>a</sup>The numbers in the parentheses represent percentage out of the four sources that are commonly identified in the source inventory and from this study.

<sup>b</sup>ND represents sources that were not detected from this study.

aromatic and alkane SOA factors accounted for 65% of OM, indicating fossil fuel combustion that was likely from motor vehicles is the largest source at Bakersfield. This finding is consistent with previous source apportionment studies at Bakersfield [Hamilton *et al.*, 2004; Kleeman *et al.*, 1999; Schauer and Cass, 2000]. Also from these studies, wood combustion was identified as a significant source only in winter, likely because residential heating (the main source of wood burning) was not in use during the early summer period [Chow *et al.*, 2006b]. However, the petroleum operation, categorized as having near-zero emissions in recent

source inventory in southern SJV (Table 3), should be added given its contribution of 14% OM.

### 3.2. Identification of Single-Particle Types

#### 3.2.1. Single-Particle NEXAFS Spectra

[43] Single-particle X-ray spectra (80 particles) were categorized into three major groups based on their spectroscopic similarities (Figure 9). To gain further insight into their source types, each group was compared to single-particle X-ray spectra for each of the 14 types of particles identified by Takahama *et al.* [2007]: Group I particles showed strong carboxylic acid group absorption at 288.7 eV. Their particle spectra were comparable to type “a” particles, likely formed from atmospheric processing, which suggests the group’s secondary origins. Group II spectra were characterized by strong absorption at 285.0 eV due to sp<sup>2</sup> bonding of soot or black carbon. Since these particles resembled Takahama’s “strongly aromatic aerosols” (e.g., type “h” particles) (Figure 9b), defined as particles that have strong absorption at 285 eV due to sp<sup>2</sup> carbon bonding, diesel exhaust was the likely origin. Group III particles showed no significant peaks for organic functional groups. The lack of a C = C peak at 285.0 eV and a C-OH peak at ~287.0 eV, which are characteristic for biomass-burning type particles, essentially excluded the possibility of Group III having a biomass burning source [Braun, 2005; Tivanski *et al.*, 2007], although the C = C peak for such particles is relatively smaller compared to that of diesel soot particles. Furthermore, high absorbance seen in the K region (at 297.4 and 299.9 eV) was consistent with dust sources, the likely origin of Group III’s particles.

#### 3.2.2. Single-Particle Mass Spectra

[44] Single-particle mass spectra for 147,357 particles were clustered (detailed in Liu *et al.* [2012]) to reveal three

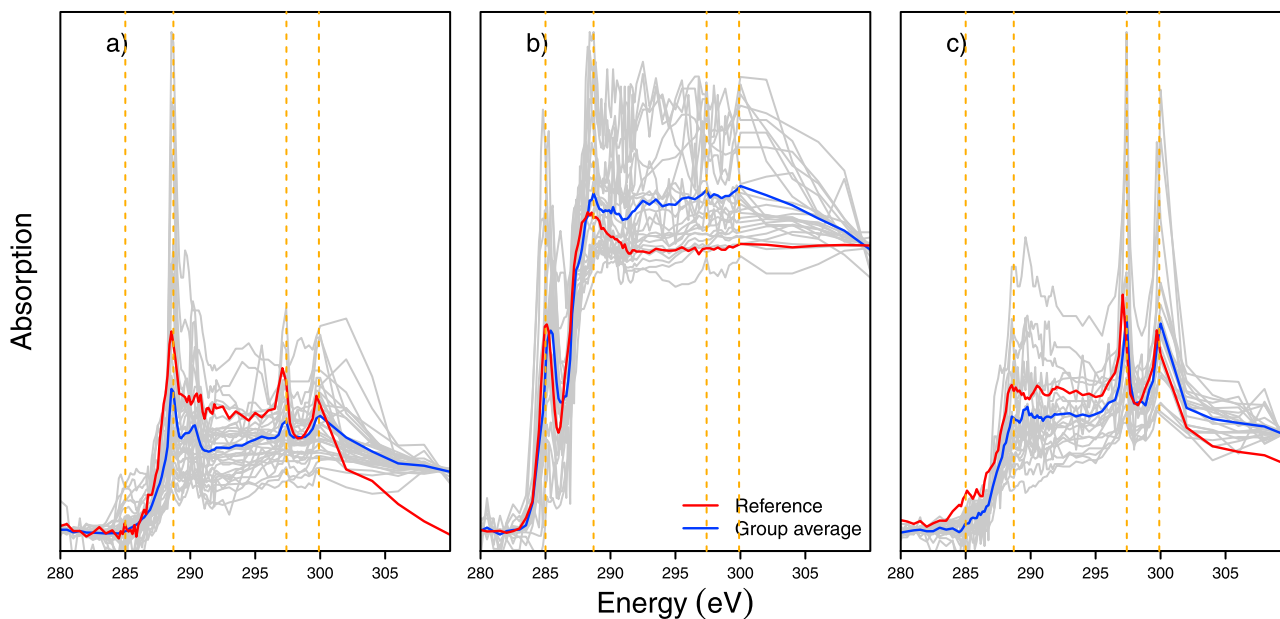


**Figure 9.** Normalized single-particle X-ray spectra for particle types: (a) Group I (35 particles), (b) Group II (24 particles), and (c) Group III (21 particles). Other identifiers include individual particle spectra (gray) and group averages (blue). For comparison, note type “a,” “h,” and “k” particles (red) (as identified by Takahama *et al.* [2007]), respectively, in Figures 9a–9c. Vertical lines (orange) in each panel represent absorptions at energies 285.0, 288.7, 297.4, and 299.9 eV.

**Table 4.** Summary of Concentration (Under the Name of the Factors), OM Fraction (in Parentheses), Oxidant, Peak Time (Under the Name of the Oxidant), O/C, Organic Functional Group (OFG) Composition, Size Range, and Source of FTIR and the AMS Factors

FTIR Factor	AMS Factor	Oxidant (Peak Time)	O/C	OFG	Size (nm)	Source
Aromatic SOA	Low O/C aromatic SOA	OH	0.36	Alkane Acid	15 0	250–900 Fossil fuel combustion
PM <sub>1</sub> : 0.61 (24%)		(0–6; 12–18)		Hydroxyl	16	(Secondary)
PM <sub>2.5</sub> : 0.77 (23%)	0.35 (9%) High O/C aromatic SOA	OH	0.68	Carbonyl Amine ON	59 10 0	200–500 Fossil fuel combustion (Secondary)
	0.64 (16%)	(18–23)				
Alkane SOA	Low O/C alkane SOA	OH	0.27	Alkane Acid	50 38	Fossil fuel combustion
PM <sub>1</sub> : 1.21 (41%)		(22–6)		Hydroxyl	7	(Secondary)
PM <sub>2.5</sub> : 1.43 (43%)	0.48 (12%) High O/C alkane SOA	O <sub>3</sub>	0.63	Carbonyl Amine ON	0 4 1	Fossil fuel combustion (Secondary)
	1.19 (30%)	(10–17)				
Nighttime OA	Nighttime OA	NO <sub>3</sub>	0.01	Alkane Acid	80 6	400–700 Fossil fuel combustion/biogenic emissions
PM <sub>1</sub> : 0.30 (10%)	0.50 (13%)	(0–6)		Hydroxyl Carbonyl Amine ON	6 0 0 8	(Primary and secondary)
PM <sub>2.5</sub> : 0.25 (8%)						
PO SOA	PO SOA	OH and/or O <sub>3</sub>	0.20	Alkane Acid	47 9	100–200 Petroleum operations
PM <sub>1</sub> : 0.42 (14%)	0.49 (13%)	(10–17)		Hydroxyl Carbonyl Amine ON	40 0 3 1	(Secondary)
PM <sub>2.5</sub> : 0.42 (13%)						
Vegetative detritus	-	-	1.09	Alkane Acid	15 1	- Resuspended dusts and plant materials
PM <sub>1</sub> : 0.29 (10%)		(12–18)		Hydroxyl Carbonyl Amine ON	71 0 13 0	(Primary)
PM <sub>2.5</sub> : 0.45 (14%)						
-	COA	-	0.05	-	-	100–200 Cooking activities
	0.29 (7%)	(12–18; 20–23)				(Primary)

single-particle clusters: Cluster I mass spectra were characterized by  $m/z$  44 and were comparable to LV-OOA spectra in the AMS database [Ulbrich *et al.*, 2009]. Cluster II particles had strong  $m/z$  43 signals, and their spectra resembled those of SV-OOA components. Cluster III spectra were characterized by  $m/z$  27, 29, 41, 55, 57, and 69, which were typical for hydrocarbon type aerosols ( $m/z$  29, 57) or cooking organic aerosols ( $m/z$  27, 41, 55, 69). This suggested that Cluster III particles likely originated from mixed local primary sources.

### 3.2.3. Single-Particle Types Compared With Bulk Source Types

[45] The “secondary” (Group I), “diesel exhaust” (Group II), and “dust” (Group III) particle types resulting from single-particle X-ray spectra broadly matched the major source types identified from bulk particle functional group factor analysis. Secondary particles accounted for 44% of

total measured particles, which was consistent with bulk particle analysis that suggested SOA was the major component of OM. Similarly, the “high  $m/z$  44” (Cluster I), “high  $m/z$  43” (Cluster II), and “mixed” (Cluster III) particle types derived from single-particle mass spectra analysis matched the major source types from the bulk particle mass spectra factor analysis. Taken together, the high  $m/z$  44 and  $m/z$  43 types accounted for 56% of identified particles, both by number and mass. Specifically, the group average high  $m/z$  44 single-particle spectrum correlated to the mass spectra for the high O/C alkane and aromatic SOA components with an  $r$  of 0.96 and 0.92, respectively. High spectral correlations were also observed for the high  $m/z$  43 type particles that correlated to the low O/C alkane SOA with  $r = 0.96$  and the mixed-type particles that correlated to COA, PO SOA, and nighttime OA with  $r = 0.86$ , 0.76, and 0.70, respectively. Agreement of

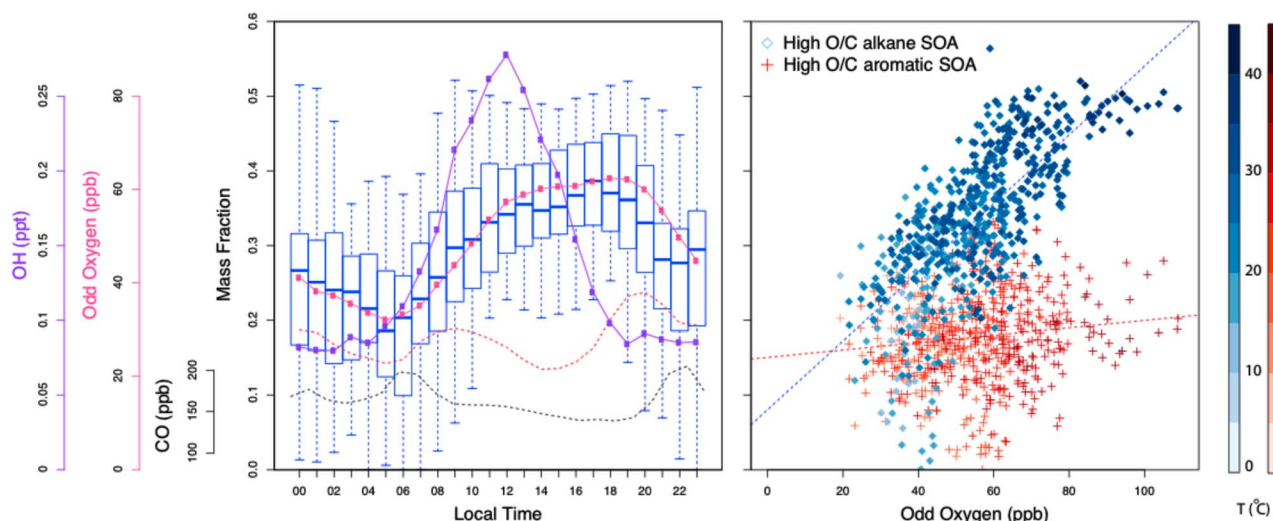


**Figure 10.** (left) Diurnal variations of mass fraction for the high O/C alkane SOA<sub>AMS</sub> factor (blue boxes), mass fraction for the high O/C aromatic SOA<sub>AMS</sub> factor (dashed red line), odd oxygen (pink), CO (black), and OH (purple). (OH radical was measured by William Brune’s research group [Ahlm *et al.*, 2012].) The horizontal bar in each box represents the median value. Upper and lower bounds of the boxes represent 25th and 75th percentiles, with whiskers extending to 5th and 95th percentiles. (right) Correlation of mass fraction of the high O/C alkane SOA<sub>AMS</sub> (blue) and high O/C aromatic SOA<sub>AMS</sub> (red) factors to odd oxygen. Darker colors indicate higher temperatures as the vertical color bars show.

single and bulk particle types speaks to the ubiquity of SOA in fine OM at Bakersfield.

## 4. Discussion

[46] The SOA components, which were derived from factor analysis, differed in mass, chemical composition, and diurnal cycle (summarized in Table 4), suggesting they were produced via distinct oxidation processes and likely favored by specific meteorological conditions. In this section, we compare the SOA components and discuss the underlying processes that likely led to their formation. Special attention is given to alkane SOA, aromatic SOA, and nighttime OA; the first two prevailed during daytime, and the last was a significant constituent at night. In addition, we discuss size distributions of SOA components, which confirm the source identification and indicate the likely formation process.

### 4.1. Contrasting Formation of Alkane and Aromatic Secondary Organic Aerosol Components

[47] The diurnal cycle for high O/C alkane SOA<sub>AMS</sub> was consistent over the course of the study, with concentrations peaking in the afternoon for 74% of the 45-day campaign (Figure 10, left). The average diurnal cycle resembled that of the odd oxygen ( $O_3 + NO_2$ ), and the factor mass fraction correlated to odd oxygen with an  $r$  of 0.70 (higher temperature associated with larger odd oxygen mixing ratios and greater factor mass fractions) (Figure 10, right), suggesting  $O_3$  either played an important role in its formation or was coproduced with alkane SOA from similar precursors on similar time scales. Good correlation of alkane SOA to odd oxygen were also found by recent model simulations even without a role for  $O_3$  in the oxidation of alkanes [Pye and

Pouliot, 2012]. The alkane SOA<sub>FTIR</sub> factor mole composition of 0.11/0.04/0.00/0.86 among carboxylic acid/hydroxyl/nonacid carbonyl/alkane groups compared well to  $C_{12}$  alkane oxidation products, with mole fractions of 0.12/0.13/0.02/0.73 for the carboxylic acid/hydroxyl/nonacid carbonyl/alkane groups [Russell *et al.*, 2011]. This composition was inferred from a two-step oxidation pathway: 1) gas-phase alkane oxidation by OH radicals to form particle-phase dihydrofuran; and 2) evaporation of dihydrofuran followed by  $O_3$  oxidation, forming carboxylic acid and alkane group dominated products [Russell *et al.*, 2011]. The products from each step likely represented first-generation and higher SOA components, respectively [Lim and Ziemann, 2005, 2009]. Therefore, that the high O/C alkane SOA<sub>AMS</sub> factor correlated with odd oxygen indicated second-generation or higher products from alkane oxidation. Neither the low O/C alkane SOA<sub>AMS</sub> factor nor the sum of the high and low O/C alkane SOA<sub>AMS</sub> factors (correlating to the alkane SOA<sub>FTIR</sub> factor,  $r = 0.74$ ) correlated to odd oxygen, indicating that the low O/C alkane SOA<sub>AMS</sub> factor may have been associated with the first step of oxidation which happened faster than  $O_3$  formation or for which  $O_3$  was not required.

[48] For the diurnal cycle of the high O/C aromatic SOA<sub>AMS</sub> factor, no consistent pattern was identified. Day-to-day variation likely resulted from the variety of the aromatic species emitted from vehicular emissions, including light aromatic hydrocarbons and polycyclic aromatic hydrocarbons (PAHs), the quantities of which are highly dependent on combusted fuels [Richter and Howard, 2000]. In contrast, alkane compounds were relatively simple in their structure and could readily be grouped into linear, branched, and cyclic alkane classes, with SOA products fairly similar among these

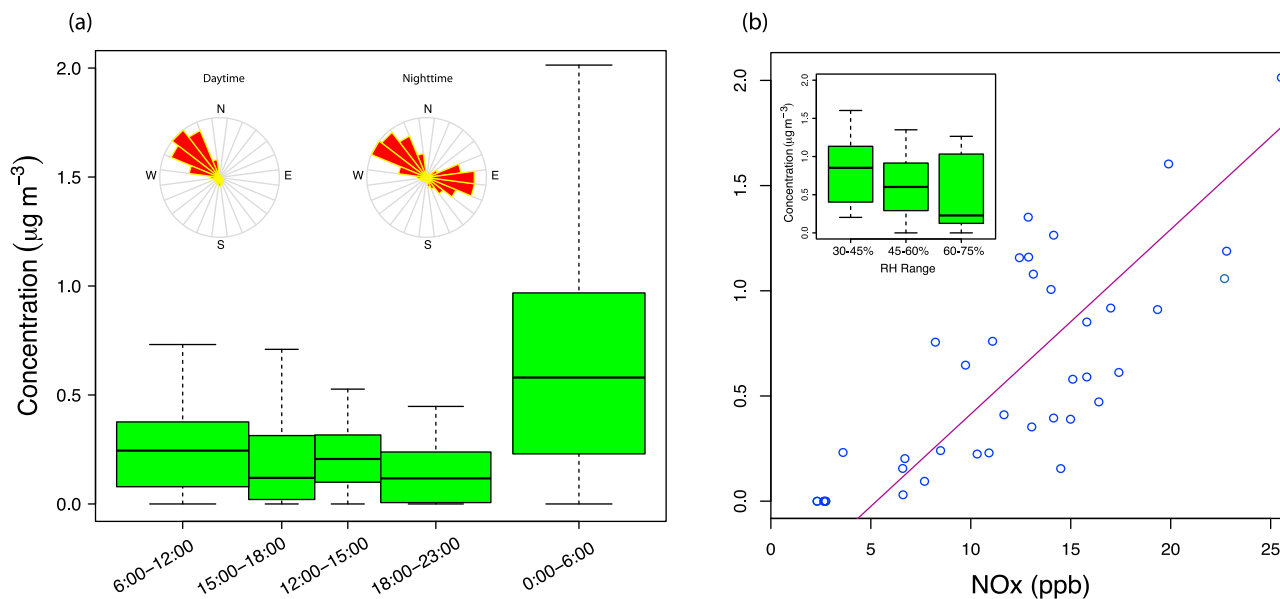


**Figure 11.** (a) Diurnal cycle of nighttime  $\text{OA}_{\text{FTIR}}$  with inner charts showing frequency of daytime and nighttime wind directions. (b) Correlation of nighttime  $\text{OA}_{\text{FTIR}}$  with  $\text{NO}_x$  for nighttime samples. The inner box plot shows dependence of factor concentration on RH, which included at least 10 points (45 points total) per bin. For each box in Figures 11a and 11b, upper and lower bounds represent 25th and 75th percentiles, and whiskers extend to 5th and 95th percentiles.

classes [Lim and Ziemann, 2009]. The mass yield of aromatic compounds may vary significantly as was found in SOA yields from naphthalene, which ranged from 2% to 22% [Shakya and Griffin, 2010] and from 19% to 74% [Chan et al., 2009] under comparable experimental conditions (i.e., OH concentration, initial hydrocarbon concentration, and initial  $\text{NO}_x$  mixing ratio). This indicated that yields of aromatic hydrocarbons were extremely sensitive to environmental conditions. In addition, SOA components from PAH oxidation have been shown to be sensitive to  $\text{NO}_x$  mixing ratios, with ring-opening compounds being major products under high  $\text{NO}_x$  conditions and ring-retaining compounds formed under low  $\text{NO}_x$  conditions [Kautzman et al., 2010].

[49] The variety of the aromatic compounds, sensitivity of their yields to the environmental conditions, and dependence of their oxidation products on  $\text{NO}_x$ , likely contributed to the variability of the diurnal cycle for the high O/C aromatic  $\text{SOA}_{\text{AMS}}$  factor. This factor's mass fraction (or mass concentration) did not correlate to odd oxygen (Figure 10), suggesting that  $\text{O}_3$  played a minor role (if any) in its formation. The aromatic  $\text{SOA}_{\text{FTIR}}$  factor, which likely represented the average composition of a variety of aromatic SOA components, was largely composed of nonacid carbonyl groups (59%), which was consistent with the OH radical oxidation products for aromatic precursors, a majority of which contain ketone groups [Esteve et al., 2003; Lee and Lane, 2009; Lee and Lane, 2010; Wang et al., 2007; Webb et al., 2006]. The similarity of the aromatic  $\text{SOA}_{\text{FTIR}}$  factor to OH oxidation products for aromatic hydrocarbons suggests that OH was the main oxidant that oxidized primary aromatic compounds to their SOA products. This observation is consistent with previous kinetic studies that showed that aromatic hydrocarbons primarily react with OH radicals in the atmosphere [Kwok et al., 1994].

[50] The functional group composition of alkane and aromatic  $\text{SOA}_{\text{FTIR}}$  factors are significantly different from the biogenic SOA factors identified in previous studies. For example, the biogenic SOA factor identified from Whistler, a remote forested site, has mole fractions of 0.44/0.25/0.16/0.10 for alkane, hydroxyl, nonacid, and carboxylic groups [Russell et al., 2011]; that is, the Whistler biogenic factor has a smaller alkane group fraction and a larger hydroxyl group fraction than the alkane  $\text{SOA}_{\text{FTIR}}$  factor. The biogenic SOA factor also has a smaller fraction of nonacid carbonyl groups than the aromatic  $\text{SOA}_{\text{FTIR}}$  factor.

#### 4.2. Nighttime Formation of Biogenic Secondary Organic Aerosols

[51] While high O/C alkane and aromatic  $\text{SOA}_{\text{AMS}}$  components peaked during the day, high concentrations (20% to 52% OM) of the nighttime OA factors were observed at night (Figure 11a). The nighttime  $\text{OA}_{\text{FTIR}}$  factor, although influenced by primary anthropogenic sources, had significant signatures of biogenic SOA. The factor composition of alkane (57% to 79% OM), organonitrate (8% to 17% OM), and nonacid carbonyl groups (0% to 8% OM) was chemically similar to  $\alpha$ -pinene and  $\beta$ -pinene SOA produced by  $\text{NO}_3$  radical oxidation. These SOA components typically comprise 63% to 68% alkane groups, 8% to 26% organonitrate groups, and 2% to 24% nonacid carbonyl groups [Hallquist et al., 1999; Wängberg et al., 1997]. Therefore, the SOA fraction of the nighttime  $\text{OA}_{\text{FTIR}}$  factor likely formed via  $\text{NO}_3$  radical oxidation. Supporting this argument is the correlation ( $r=0.5$ ) of nighttime  $\text{OA}_{\text{FTIR}}$  with nitrated organosulfates (e.g.,  $\text{C}_{10}\text{H}_{16}\text{NO}_7\text{S}^-$ ,  $\text{C}_9\text{H}_{14}\text{NO}_8\text{S}^-$ , and  $\text{C}_{10}\text{H}_{16}\text{NO}_{10}\text{S}^-$  ions measured by UPLC/ESI-HR-Q-TOFMS), the most abundant organosulfate compound class (observed at the Bakersfield site) that is likely produced from  $\text{NO}_3$  radical oxidation of

**Table 5.** Mean Concentration, Variability, and Fraction of Variability Explained by the AMS Factors for the OM Sections

	OM <sub>30–100</sub>	OM <sub>100–200</sub>	OM <sub>200–300</sub>	OM <sub>300–400</sub>	OM <sub>400–500</sub>	OM <sub>500–600</sub>	OM <sub>600–700</sub>	OM <sub>700–800</sub>	OM <sub>800–900</sub>	OM <sub>900–1000</sub>
Mean concentration ( $\mu\text{g m}^{-3}$ )	0.12	0.55	0.30	0.20	0.11	0.07	0.04	0.03	0.01	0.01
Variability (standard deviation) ( $\mu\text{g m}^{-3}$ )	0.08	0.32	0.22	0.17	0.09	0.06	0.04	0.03	0.02	0.01
Ratio of variability to mean	0.69	0.58	0.71	0.83	0.83	0.83	0.95	1.05	1.20	1.50
Fraction of variability explained ( $r^2$ )										
Low O/C aromatic SOA	0.03	0.04	0.36	0.44	0.49	0.45	0.43	0.45	0.38	0.35
High O/C aromatic SOA	0.02	0.28	0.69	0.61	0.35	0.15	0.10	0.12	0.13	0.14
Low O/C alkane SOA	0.01	0.26	0.60	0.53	0.44	0.30	0.27	0.27	0.24	0.25
High O/C alkane SOA	0.01	0.16	0.67	0.64	0.31	0.12	0.10	0.13	0.14	0.15
Nighttime OA	0.00	0.04	0.05	0.12	0.45	0.67	0.66	0.56	0.44	0.31
PO SOA	0.25	0.53	0.33	0.20	0.08	0.02	0.01	0.02	0.03	0.03
COA	0.21	0.48	0.07	0.01	0.00	0.00	0.00	0.00	0.00	0.00

$\alpha$ -pinene and limonene-like monoterpenes (e.g., myrcene) under dark conditions [Surratt *et al.*, 2008].

[52] As described in section 3.1, easterly downslope winds prevailed at night, which likely carried biogenic VOCs to the sampling site. Biogenic VOCs (e.g., terpenes) typically contain one or more carbon-carbon double bonds, highly chemically active and readily oxidized typically by  $\text{O}_3$  and  $\text{NO}_3$  radicals under nighttime conditions. While some background  $\text{O}_3$  was still detected at night ( $\sim 10$  ppb), no correlation was observed between the nighttime  $\text{OA}_{\text{FTIR}}$  factor and the  $\text{O}_3$  concentration, indicating  $\text{O}_3$  may not play a major role in formation of nighttime  $\text{OA}_{\text{FTIR}}$ . However, background  $\text{O}_3$  could react with  $\text{NO}_2$  to generate  $\text{NO}_3$  radicals and could also convert  $\text{NO}$  to  $\text{NO}_2$  to prevent loss of  $\text{NO}_3$  radicals by reacting with  $\text{NO}$ . The nighttime  $\text{OA}_{\text{FTIR}}$  factor correlated to nighttime  $\text{NO}_x$  (Figure 11b), which is the precursor of  $\text{NO}_3$  radicals, confirming that nighttime  $\text{OA}_{\text{FTIR}}$  was likely formed by  $\text{NO}_3$  radical oxidation. Rollins *et al.* [2012] estimated that 1/3 of OM increase at night was accounted for by organonitrate group-containing molecules, which is consistent with the nighttime formation mechanism of the nighttime  $\text{OA}_{\text{FTIR}}$  factor. Moreover, the nighttime  $\text{OA}_{\text{FTIR}}$  factor accounted for 50% to 80% of the observed organonitrate group mass, which is consistent with an expected higher organonitrate group yield from  $\text{NO}_3$  oxidation reactions than that from OH radical and  $\text{O}_3$  oxidation processes. Additionally, lower concentrations of nighttime  $\text{OA}_{\text{FTIR}}$  were associated with high RH (Figure 11b), which is consistent with the loss of  $\text{NO}_3$  radicals under high RH conditions (shifting the reaction  $\text{NO}_3 + \text{NO}_2 = \text{N}_2\text{O}_5$  to the right through  $\text{N}_2\text{O}_5$  uptake under high RH). Although alkane and aromatic hydrocarbons coexisted with biogenic VOCs at night, their oxidation rate constants for  $\text{NO}_3$  radicals were typically less than  $10^{-16}$  and  $10^{-15}$   $\text{cm}^3$  molecule $^{-1}$  s $^{-1}$ , respectively [Atkinson and Arey, 2003]. These rate constants were  $10^3$  to  $10^6$  times smaller than rate constants of the biogenic hydrocarbons (oxidation by  $\text{NO}_3$  radicals), which typically ranged from  $10^{-10}$  to  $10^{-12}$   $\text{cm}^3$  molecule $^{-1}$  s $^{-1}$  [Atkinson and Arey, 2003]. Therefore,  $\text{NO}_3$  radicals mainly reacted with biogenic VOCs, forming biogenic SOA components with organonitrate functional groups in the nighttime atmosphere.

[53] Compared to the biogenic SOA factors identified at Whistler (British Columbia, at 1020 m above sea level) [Schwartz *et al.*, 2010], the nighttime  $\text{OA}_{\text{FTIR}}$  factor had significantly larger contribution of organonitrate groups. This difference likely arises from distinct oxidation conditions:  $\text{O}_3$  or OH radical oxidation under low  $\text{NO}_x$  (1.5 ppb) at Whistler and  $\text{NO}_3$  radical oxidation under high  $\text{NO}_x$  (15 ppb at night) at Bakersfield.

### 4.3. Insights of SOA Formation From Factor Size Distribution

[54] Time series of the OM factors were correlated to time series of OM particle size sections ( $\text{OM}_{30–100}$ ,  $\text{OM}_{100–200}$ ,  $\text{OM}_{200–300}$ ,  $\text{OM}_{300–400}$ ,  $\text{OM}_{400–500}$ ,  $\text{OM}_{500–600}$ ,  $\text{OM}_{600–700}$ ,  $\text{OM}_{700–800}$ ,  $\text{OM}_{800–900}$ ,  $\text{OM}_{900–1000}$ ) derived from the AMS TOF mode measurements, resulting in a set of correlation coefficients for each factor. The square of the correlation coefficient ( $r^2$ ) between an OM section and a factor represents the fraction of variability of an OM section that could be explained by variability of the factor [Rodgers and Nicewander, 1988]. The mean and variability (standard deviation) for the OM sections were comparable (Table 5), suggesting that most of the OM concentration was controlled by OM variability. Similarly, the factor concentration was controlled by variability in the factor concentration. Therefore, high  $r^2$  between an OM section and a factor suggests that the mass of the OM section was likely accounted for by the factor, i.e., a majority of the factor mass likely distributed in the same size range as the OM section. For this reason, the  $r^2$  distribution (versus size) for each factor represents the factor mass size distribution to a great extent. Factor mass size distribution estimated from this approach can be validated by size distribution estimated from a marker-based method (e.g., size distribution of  $m/z$  44 represents size distribution of SOA), which has proven to be approximately accurate [Ulbrich *et al.*, 2012].

[55] Variability of OM in 200 nm to 500 nm sized particles was accounted for by the high O/C alkane and aromatic SOA factors (Figure 12a), suggesting that the high O/C factors peaked in 200 nm to 500 nm size range. Mass of fragment  $\text{CO}_2^+$  ( $m/z$  44), largely accounted for by high O/C alkane SOA (55%) and high O/C aromatic SOA (30%) factors, peaked in the 150 nm to 500 nm size range, which agreed well with  $r^2$  distributions for the two high O/C factors. These peak size ranges are comparable to those for the OOA factor identified from Mexico City measurements using 3-D factorization analysis [Ulbrich *et al.*, 2012]. Oxidized components enriched in 200 nm to 500 nm sized particles typically form by condensation of gas-phase secondary organic species, because these particles provide most of the surface area that mass transfer mainly occurs in this size range [Seinfeld and Pandis, 2006]. In addition, oxidized components in 200 nm to 500 nm sized particles are often associated with high  $\text{O}_3$  mixing ratios [Alfarra *et al.*, 2004; Liu *et al.*, 2008; Zhang *et al.*, 2005], suggesting that the high O/C factors were produced during photochemical processes. Note that  $r^2$  size distributions of the

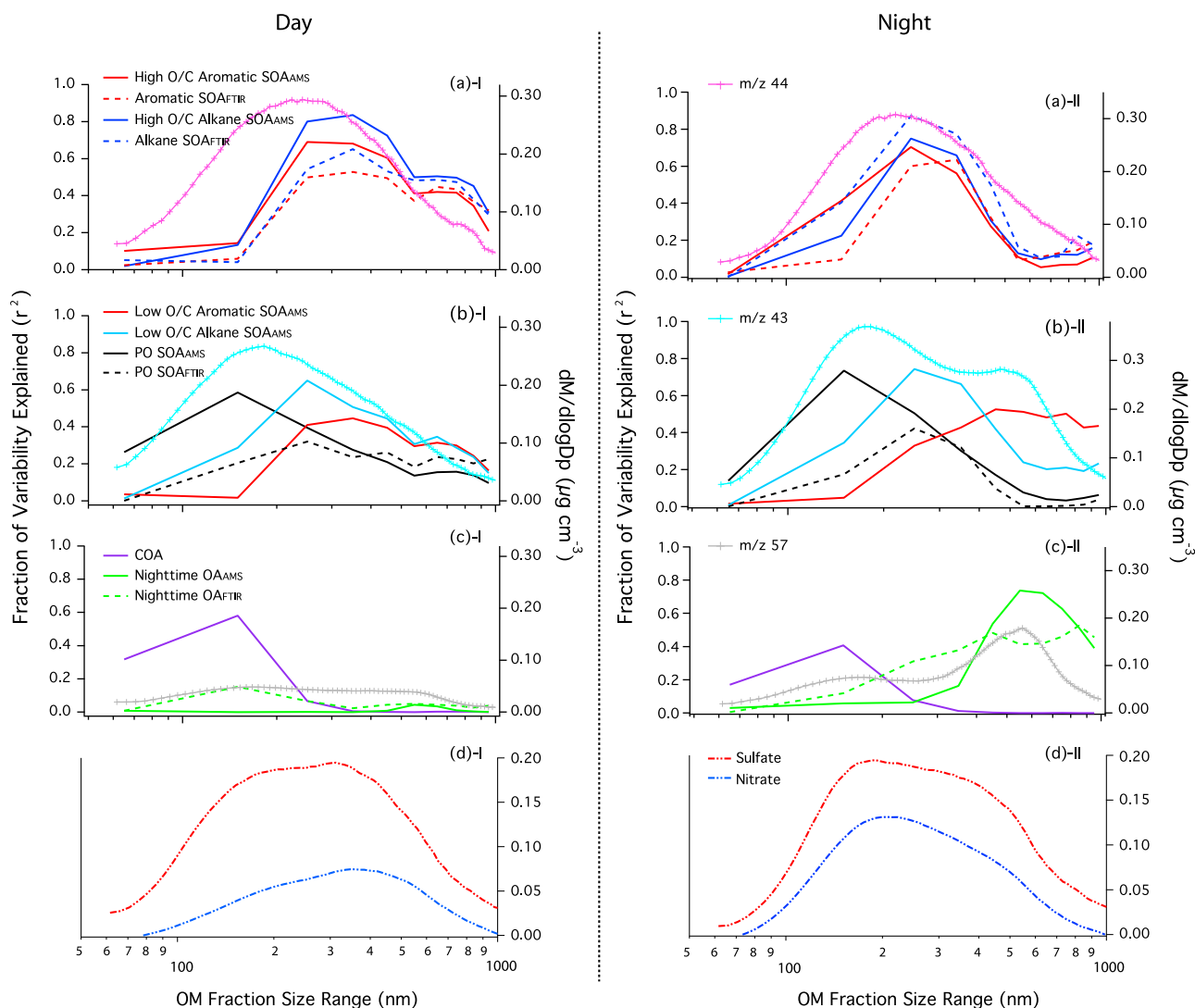


**Figure 12.** Size distributions of  $r^2$  (fraction of variability explained) for FTIR and AMS factors (left axes) and mass size distributions of (a) m/z 44, (b) m/z 57, (c) m/z 43, and (d) sulfate and nitrate (right axes) for (left) daytime and (right) nighttime measurements. Legends for the factors and AMS-measured components are displayed on the left and right sides of the graphs, respectively.

high O/C factors shifted 50 nm (daytime) and 20 nm (nighttime) toward larger sized particles compared to the m/z 44 size distribution, a difference likely caused by variation of non-m/z 44 fragments in the high O/C factors that underwent different atmospheric processes compared to the processes experienced by fragment m/z 44. Larger daytime shifts reflect more complex processes, which could also explain the shoulder at 600 nm to 900 nm of daytime  $r^2$  distributions. Low O/C alkane and aromatic SOA factors had similar  $r^2$  size distributions compared to those for the high O/C factors, except the low O/C alkane SOA was broadly distributed (250 to 900 nm) (Figure 12b). This likely resulted from the low O/C alkane SOA's temperature-driven condensation at night [Lanz *et al.*, 2007; Ng *et al.*, 2010], as daily temperatures fluctuated widely (10–20°C). The  $r^2$  of another low O/C factor, PO SOA, peaked in the 100 nm to 200 nm size range. Fragment m/z 43 (72%  $\text{C}_2\text{H}_3\text{O}^+$  and 28%  $\text{C}_3\text{H}_7^+$ ) was representative of low O/C factors. Daytime size distribution of m/z 43 peaked in the 100 nm to 600 nm size range, as was

consistent with size distributions of low O/C alkane SOA, low O/C aromatic SOA, and PO SOA factors. A distinct mode of m/z 43 at 400 nm to 700 nm occurred at night, likely a contribution of  $\text{C}_3\text{H}_7^+$  from primary emissions.

[56] The size distribution of  $r^2$  of the nighttime OA factor peaked in the 400 nm to 700 nm size range at night (Figure 12c). This size range largely overlapped the larger mode in nighttime size distribution of m/z 57, which was expected because 60% of m/z 57 mass fragment was attributed to the nighttime OA factor. The 400 nm to 700 nm mode was not present in the size distribution of SOA components (such as fragment m/z 44, sulfate, and nitrate, Figure 12), suggesting that nighttime OM<sub>400–700</sub> was likely associated with primary emissions. A likely primary source was vehicular emissions. Although fresh exhaust particles are typically smaller than 100 nm, a mode at 550 nm was observed from chase studies using AMS [Canagaratna *et al.*, 2004]. In addition, Kleeman *et al.* [2009] attributed a significant mass of particles (560–1000 nm) to diesel fuel and gasoline

combustion sources at the same site. Another source of particles in this mode could be vegetative detritus, which likely existed as large particles (section 3.1). SOA produced at night (e.g., biogenic SOA) could condense on large primary particles to form internal mixtures. Therefore, the nighttime OA factor, which included a mixture of primary and secondary signatures, likely represented a mixture of primary hydrocarbons and condensed secondary biogenic SOA components formed by NO<sub>3</sub> oxidation.

[57] The size distribution of  $r^2$  for the COA factor peaked in 100 nm to 200 nm, a size range consistent with primarily emitted particles from meat charbroiling and frying activities [Hildemann *et al.*, 1991; Wallace *et al.*, 2004; Kleeman *et al.*, 2009; Allan *et al.*, 2010; Zhang *et al.*, 2007], which agreed with the low O/C (0.04) for this factor.

## 5. Conclusions

[58] Summertime measurements suggested that organic mass comprised the major component of fine aerosol particles at Bakersfield in the San Joaquin Valley. On average, OM in PM<sub>1</sub> and PM<sub>2.5</sub> was 2.42 and 3.23  $\mu\text{g m}^{-3}$ , respectively. PMF analysis was applied to the FTIR and AMS measurements, resulting in very high agreement between the two sets of independently derived factors, both of which suggested that SOA components accounted for 80% to 90% of fine particle OM. The high O/C AMS factors were chemically similar, so that external source marker were needed to link them to specific sources; whereas the FTIR factors had distinct infrared spectra that could be used as references for future studies when source marker measurements are not available. Among the PMF-derived components, vehicular emission oxidation products, including the alkane and aromatic SOA factors, constituted 65% OM, whereas nighttime organic aerosols (the nighttime OA factor), a mixture of POA and SOA that likely originated from biogenic emissions, accounted for a relatively small fraction on average (10% OM), although it was higher at night (20% OM).

[59] Potential formation mechanisms of the SOA components were discussed. Anthropogenic SOA components mainly formed during daytime. The alkane SOA consisted of alkane and carboxylic acid groups, consistent with the composition expected for oxidation products of C<sub>12</sub>–C<sub>25</sub> alkanes. Furthermore, organic mass fraction of alkane SOA covaried and correlated with odd oxygen, providing evidence for the ozone-driven formation of alkane SOA, a mechanism derived from laboratory studies. In contrast, aromatic SOA did not correlate with ozone. This component was largely composed of nonacid carbonyl groups, which is consistent with oxidation products formed from OH radical-driven reactions for aromatic hydrocarbons and, therefore, indicates formation by this process. The nighttime organic aerosol component accounted for 50% to 80% of organonitrate group mass during the project; the secondary fraction of nighttime OA likely formed from oxidation of biogenic precursors (e.g., terpenes) by nitrate radicals during nighttime hours.

[60] Not only did anthropogenic and biogenic SOA components differ in composition, they also differed in size: namely, oxidized alkane and aromatic SOA components was largely distributed in 200 nm to 500 nm sized particles, suggesting that they were formed from condensation of gas-phase oxidation products, while biogenic SOA was in

400 nm to 700 nm sized particles at night, likely due to condensation of biogenic SOA on large primary particles.

[61] We also identified aerosols likely emitted from local petroleum operations and cooking activities, which were likely in particles smaller than 200 nm. Though these sources were negligibly small in the emission inventory for the Bakersfield site, they accounted for 13% and 7% of the PM<sub>1</sub> organic mass, respectively.

[62] Overall, this work demonstrates that OOA components identified from factor analysis can be linked to SOA formed by different oxidants and precursors mainly from gasoline and diesel fuel combustion emissions with minor contributions from petroleum operation and biogenic sources. In addition, these SOA components were enriched at particular sizes. We conclude that SOA accounts for a major fraction of summertime OM, even in areas close to urban sources. This result provides a benefit to the SJV community because it identifies the need for regulating vehicular emissions as the largest source of PM<sub>1</sub> in summertime.

[71] **Acknowledgments.** The authors appreciate California Air Resources Board (CARB) for funding this work (contract 09–328). We thank the CalNex-SJV research team for the cooperation and contribution to this paper. Particularly, we acknowledge Ron Cohen at University of California, Berkeley, and his group members Sally Pusede and Ellie Browne for providing the NO<sub>x</sub> measurements and William Brune at Pennsylvania State University for providing OH measurements. The authors are also grateful to John Karlik and the Kern County University of California Cooperative Extension staff for their generous help during the measurements. The statements and conclusions in this paper are those of the researchers (contractor) and not necessarily those of CARB. The mention of commercial products, their source, or their use in connection with material reported herein is not to be construed as actual or implied endorsement of such products. The U.S. Environmental Protection Agency through its Office of Research and Development partially funded and collaborated in the research described here under contract EP-D-10-070 to Alion Science and Technology. The manuscript is subjected to external peer review and has been cleared for publication. Mention of trade names or commercial products does not constitute an endorsement or recommendation for use.

## References

- Ahlm, L., et al. (2012), Formation and growth of ultrafine particles from secondary sources in Bakersfield, California, *J. Geophys. Res.*, *117*, D00V08, doi:10.1029/2011JD017144.
- Aiken, A. C., et al. (2008), O/C and OM/OC ratios of primary, secondary, and ambient organic aerosols with high-resolution time-of-flight aerosol mass spectrometry, *Environ. Sci. Technol.*, *42*(12), 4478–4485, doi:10.1021/es703009q.
- Alfarra, M. R., et al. (2004), Characterization of urban and rural organic particulate in the lower Fraser valley using two aerodyne aerosol mass spectrometers, *Atmos. Environ.*, *38*(34), 5745–5758, doi:10.1016/j.atmosenv.2004.01.054.
- Allan, J. D., P. I. Williams, W. T. Morgan, C. L. Martin, M. J. Flynn, J. Lee, E. Nemitz, G. J. Phillips, M. W. Gallagher, and H. Coe (2010), Contributions from transport, solid fuel burning and cooking to primary organic aerosols in two UK cities, *Atmos. Chem. Phys.*, *10*(2), 647–668, doi:10.5194/acp-10-647-2010.
- Atkinson, R., and J. Arey (2003), Atmospheric degradation of volatile organic compounds, *Chem. Rev.*, *103*(12), 4605–4638, doi:10.1021/cr0206420.
- Bianchi, G., A. Gamba, R. Limiroli, N. Pozzi, R. Elster, F. Salamini, and D. Bartels (1993), The unusual sugar composition in leaves of the resurrection plant *myrothamnus-flabellifolia*, *Physiol. Plant.*, *87*(2), 223–226, doi:10.1111/j.1399-3054.1993.tb00146.x.
- Braun, A. (2005), Carbon speciation in airborne particulate matter with C (1 s) NEXAFS spectroscopy, *J. Environ. Monit.*, *7*(11), 1059–1065, doi:10.1039/b508910g.
- Canagaratna, M. R., et al. (2004), Chase studies of particulate emissions from in-use New York City vehicles, *Aerosol Sci. Technol.*, *38*(6), 555–573, doi:10.1080/02786820490465504.
- Canagaratna, M. R., et al. (2007), Chemical and microphysical characterization of ambient aerosols with the aerodyne aerosol mass spectrometer, *Mass Spectrom. Rev.*, *26*(2), 185–222, doi:10.1002/mas.20115.

- Cass, G. R. (1998), Organic molecular tracers for particulate air pollution sources, *Trends Analyt. Chem.*, 17(6), 356–366, doi:10.1016/S0165-9936(98)00040-5.
- Chan, A. W. H., K. E. Kautzman, P. S. Chhabra, J. D. Surratt, M. N. Chan, J. D. Crouse, A. Kuerten, P. O. Wennberg, R. C. Flagan, and J. H. Seinfeld (2009), Secondary organic aerosol formation from photooxidation of naphthalene and alkylnaphthalenes: Implications for oxidation of intermediate volatility organic compounds (IVOCs), *Atmos. Chem. Phys.*, 9(9), 3049–3060, doi:10.5194/acp-9-3049-2009.
- Chow, J. C., J. G. Watson, Z. Q. Lu, D. H. Lowenthal, C. A. Frazier, P. A. Solomon, R. H. Thuillier, and K. Magliano (1996), Descriptive analysis of PM<sub>2.5</sub> and PM<sub>10</sub> at regionally representative locations during sjvaqs/auspex, *Atmos. Environ.*, 30(12), 2079–2112, doi:10.1016/1352-2310(95)00402-5.
- Chow, J. C., J. G. Watson, L. L. Ashbaugh, and K. L. Magliano (2003), Similarities and differences in PM<sub>10</sub> chemical source profiles for geological dust from the San Joaquin Valley, California, *Atmos. Environ.*, 37(9–10), 1317–1340, doi:10.1016/S1352-2310(02)01021-X.
- Chow, J. C., J. G. Watson, D. H. Lowenthal, L. W. A. Chen, and K. L. Magliano (2006a), Particulate carbon measurements in California's San Joaquin Valley, *Chemosphere*, 62(3), 337–348, doi:10.1016/j.chemosphere.2005.04.094.
- Chow, J. C., L. W. A. Chen, J. G. Watson, D. H. Lowenthal, K. A. Magliano, K. Turkiewicz, and D. E. Lehrman (2006b), PM<sub>2.5</sub> chemical composition and spatiotemporal variability during the California Regional PM<sub>10</sub>/PM<sub>2.5</sub> Air Quality Study (CRPAQS), *J. Geophys. Res.*, 111, D10S04, doi:10.1029/2005JD006457.
- Claeys, M., et al. (2007), Hydroxydicarboxylic acids: Markers for secondary organic aerosol from the photooxidation of alpha-pinene, *Environ. Sci. Technol.*, 41(5), 1628–1634, doi:10.1021/es062181.
- Cross, E. S., J. G. Slowik, P. Davidovits, J. D. Allan, D. R. Worsnop, J. T. Jayne, D. K. Lewis, M. Canagaratna, and T. B. Onasch (2007), Laboratory and ambient particle density determinations using light scattering in conjunction with aerosol mass spectrometry, *Aerosol Sci. Technol.*, 41(4), 343–359, doi:10.1080/02786820701199736.
- Day, D. A., S. Liu, L. M. Russell, and P. J. Ziemann (2010), Organonitrate group concentrations in submicron particles with high nitrate and organic fractions in coastal southern California, *Atmos. Environ.*, 44(16), 1970–1979, doi:10.1016/j.atmosenv.2010.02.045.
- DeCarlo, P. F., J. G. Slowik, D. R. Worsnop, P. Davidovits, and J. L. Jimenez (2004), Particle morphology and density characterization by combined mobility and aerodynamic diameter measurements. Part I: Theory, *Aerosol Sci. Technol.*, 38(12), 1185–1205, doi:10.1080/027868290903907.
- Esteve, W., H. Budzinski, and E. Villenave (2003), Heterogeneous reactivity of OH radicals with phenanthrene, *Polycyclic Aromatic Compounds*, 23(5), 441–456, doi:10.1080/714040938.
- Fatemi, S. M., and B. Y. Jamaloee (2011), Preliminary considerations on the application of toe-to-heel steam flooding (THSF): Injection well-producer well configurations, *Chem. Eng. Res. Des.*, 89(11), 2365–2379, doi:10.1016/j.cherd.2011.03.007.
- Gilardoni, S., S. Liu, S. Takahama, L. M. Russell, J. D. Allan, R. Steinbrecher, J. L. Jimenez, P. F. De Carlo, E. J. Dunlea, and D. Baumgardner (2009), Characterization of organic ambient aerosol during MIRAGE 2006 on three platforms, *Atmos. Chem. Phys.*, 9(15), 5417–5432, doi:10.5194/acp-9-5417-2009.
- Goldstein, A. H., and I. E. Galbally (2007), Known and unexplored organic constituents in the earth's atmosphere, *Environ. Sci. Technol.*, 41(5), 1514–1521, doi:10.1021/es072476p.
- Goldstein, A. H., C. D. Koven, C. L. Heald, and I. Y. Fung (2009), Biogenic carbon and anthropogenic pollutants combine to form a cooling haze over the southeastern United States, *Proc. Natl. Acad. Sci. U. S. A.*, 106(22), 8835–8840, doi:10.1073/pnas.0904128106.
- Gray, H. A., G. R. Cass, J. J. Huntzicker, E. K. Heyerdahl, and J. A. Rau (1986), Characteristics of atmospheric organic and elemental carbon particle concentrations in Los Angeles, *Environ. Sci. Technol.*, 20(6), 580–589, doi:10.1021/es00148a006.
- Grosjean, D. (1984), Particulate carbon in Los Angeles air, *Sci. Total Environ.*, 32(2), 133–145, doi:10.1016/0048-9697(84)90126-8.
- Hallquist, M., I. Wängberg, E. Ljungstrom, I. Barnes, and K. H. Becker (1999), Aerosol and product yields from NO<sub>3</sub> radical-initiated oxidation of selected monoterpenes, *Environ. Sci. Technol.*, 33(4), 553–559, doi:10.1021/es980292s.
- Hamilton, J. F., P. J. Webb, A. C. Lewis, J. R. Hopkins, S. Smith, and P. Davy (2004), Partially oxidised organic components in urban aerosol using GCXGC-TOF/MS, *Atmos. Chem. Phys.*, 4, 1279–1290, doi:10.5194/acp-4-1279-2004.
- Han, J. S., K. J. Moon, S. J. Lee, Y. J. Kim, S. Y. Ryu, S. S. Cliff, and S. M. Yi (2006), Size-resolved source apportionment of ambient particles by positive matrix factorization at Gosan background site in East Asia, *Atmos. Chem. Phys.*, 6, 211–223, doi:10.5194/acp-6-211-2006.
- Hatakeyama, S., T. Tanonaka, J. H. Weng, H. Bandow, H. Takagi, and H. Akimoto (1985), Ozone-cyclohexene reaction in air: Quantitative analysis of particulate products and the reaction mechanism, *Environ. Sci. Technol.*, 19(10), 935–942, doi:10.1021/es00140a008.
- Hatakeyama, S., M. Ohno, J. H. Weng, H. Takagi, and H. Akimoto (1987), Mechanism for the formation of gaseous and particulate products from ozone-cycloalkene reactions in air, *Environ. Sci. Technol.*, 21(1), 52–57, doi:10.1021/es00155a005.
- Hawkins, L. N., and L. M. Russell (2010), Oxidation of ketone groups in transported biomass burning aerosol from the 2008 Northern California Lightning Series fires, *Atmos. Environ.*, 44(34), 4142–4154, doi:10.1016/j.atmosenv.2010.07.036.
- He, L. Y., M. Hu, X. F. Huang, B. D. Yu, Y. H. Zhang, and D. Q. Liu (2004), Measurement of emissions of fine particulate organic matter from Chinese cooking, *Atmos. Environ.*, 38(38), 6557–6564, doi:10.1016/j.atmosenv.2004.08.034.
- He, L. Y., Y. Lin, X. F. Huang, S. Guo, L. Xue, Q. Su, M. Hu, S. J. Luan, and Y. H. Zhang (2010), Characterization of high-resolution aerosol mass spectra of primary organic aerosol emissions from Chinese cooking and biomass burning, *Atmos. Chem. Phys.*, 10(23), 11,535–11,543, doi:10.5194/acp-10-11535-2010.
- Heald, C. L., J. H. Kroll, J. L. Jimenez, K. S. Docherty, P. F. DeCarlo, A. C. Aiken, Q. Chen, S. T. Martin, D. K. Farmer, and P. Artaxo (2010), A simplified description of the evolution of organic aerosol composition in the atmosphere, *Geophys. Res. Lett.*, 37, L08803, doi:10.1029/2010GL042737.
- Heintzenberg, J., D. C. Covert, and R. Van Dingenen (2000), Size distribution and chemical composition of marine aerosols: A compilation and review, *Tellus, Ser. B*, 52(4), 1104–1122, doi:10.1034/j.1600-0889.2000.00136.x.
- Hildemann, L. M., G. R. Markowski, M. C. Jones, and G. R. Cass (1991), Submicrometer aerosol mass distributions of emissions from boilers, fireplaces, automobiles, diesel trucks, and meat cooking operations, *Aerosol Sci. Technol.*, 14(1), 138–152, doi:10.1080/02786829108959478.
- Hoppel, W. A., J. W. Fitzgerald, G. M. Frick, R. E. Larson, and E. J. Mack (1990), Aerosol size distributions and optical properties found in the marine boundary layer over the Atlantic Ocean, *J. Geophys. Res.*, 95(D4), 3659–3686, doi:10.1029/JD095iD04p03659.
- Huang, X.-F., et al. (2010), Highly time-resolved chemical characterization of atmospheric submicron particles during 2008 Beijing Olympic Games using an Aerodyne High Resolution Aerosol Mass Spectrometer, *Atmos. Chem. Phys.*, 10, 8933–8945, doi:10.5194/acp-10-8933-2010.
- Jaoui, M., T. E. Kleindienst, M. Lewandowski, and E. O. Edney (2004), Identification and quantification of aerosol polar oxygenated compounds bearing carboxylic or hydroxyl groups. 1. Method development, *Anal. Chem.*, 76(16), 4765–4778, doi:10.1021/ac049919h.
- Jaoui, M., E. O. Edney, T. E. Kleindienst, M. Lewandowski, J. H. Offenberg, J. D. Surratt, and J. H. Seinfeld (2008), Formation of secondary organic aerosol from irradiated alpha-pinene/toluene/NO<sub>x</sub> mixtures and the effect of isoprene and sulfur dioxide, *J. Geophys. Res.*, 113, D09303, doi:10.1029/2007JD009426.
- Jayne, J. T., D. C. Leard, X. F. Zhang, P. Davidovits, K. A. Smith, C. E. Kolb, and D. R. Worsnop (2000), Development of an aerosol mass spectrometer for size and composition analysis of submicron particles, *Aerosol Sci. Technol.*, 33(1–2), 49–70, doi:10.1080/027868200410840.
- Jimenez, J. L., et al. (2009), Evolution of organic aerosols in the atmosphere, *Science*, 326(5959), 1525–1529, doi:10.1126/science.1180353.
- Karanasiou, A. A., P. A. Siskos, and K. Eleftheriadis (2009), Assessment of source apportionment by Positive Matrix Factorization analysis on fine and coarse urban aerosol size fractions, *Atmos. Environ.*, 43(21), 3385–3395, doi:10.1016/j.atmosenv.2009.03.051.
- Kautzman, K. E., J. D. Surratt, M. N. Chan, A. W. H. Chan, S. P. Hersey, P. S. Chhabra, N. F. Dalleska, P. O. Wennberg, R. C. Flagan, and J. H. Seinfeld (2010), Chemical composition of gas- and aerosol-phase products from the photooxidation of naphthalene, *J. Phys. Chem. A*, 114(2), 913–934, doi:10.1021/jp908530s.
- Kawamura, K., M. Narukawa, S.-M. Li, and L. A. Barrie (2007), Size distributions of dicarboxylic acids and inorganic ions in atmospheric aerosols collected during polar sunrise in the Canadian high Arctic, *J. Geophys. Res.*, 112, D10307, doi:10.1029/2006JD008244.
- Khalaf, F., P. Litherly, and V. Anderlini (1982), Vanadium as a tracer of oil pollution in the sediments of Kuwait, *Hydrobiologia*, 91, 147–154.
- Kirchstetter, T. W., B. C. Singer, R. A. Harley, G. R. Kendall, and J. M. Hesson (1999), Impact of California reformulated gasoline on motor vehicle emissions. 2. Volatile organic compound speciation and reactivity, *Environ. Sci. Technol.*, 33(2), 329–336, doi:10.1021/es980374g.
- Kittelson, D. B. (1998), Engines and nanoparticles: A review, *J. Aerosol Sci.*, 29(5–6), 575–588, doi:10.1016/S0021-8502(97)10037-4.

- Kleeman, M. J., L. S. Hughes, J. O. Allen, and G. R. Cass (1999), Source contributions to the size and composition distribution of atmospheric particles: Southern California in September 1996, *Environ. Sci. Technol.*, *33*(23), 4331–4341, doi:10.1021/es990632p.
- Kleeman, M. J., S. G. Riddle, M. A. Robert, C. A. Jakober, P. M. Fine, M. D. Hays, J. J. Schauer, and M. P. Hannigan (2009), Source apportionment of fine (PM<sub>1.8</sub>) and ultrafine (PM<sub>0.1</sub>) airborne particulate matter during a severe winter pollution episode, *Environ. Sci. Technol.*, *43*(2), 272–279, doi:10.1021/es800400m.
- Kleindienst, T. E., M. Jaoui, M. Lewandowski, J. H. Offenberg, C. W. Lewis, P. V. Bhave, and E. O. Edney (2007), Estimates of the contributions of biogenic and anthropogenic hydrocarbons to secondary organic aerosol at a southeastern US location, *Atmos. Environ.*, *41*(37), 8288–8300, doi:10.1016/j.atmosenv.2007.06.045.
- Kleindienst, T. E., M. Jaoui, M. Lewandowski, J. H. Offenberg, and K. S. Docherty (2012), The formation of SOA and chemical tracer compounds from the photooxidation of naphthalene and its methyl analogs in the presence and absence of nitrogen oxides, *Atmos. Chem. Phys. Discuss.*, *12*, 12163–12201, doi:10.5194/acpd-12-12163-2012.
- Kwok, E. S. C., W. P. Harger, J. Arey, and R. Atkinson (1994), Reactions of gas-phase phenanthrene under simulated atmospheric conditions, *Environ. Sci. Technol.*, *28*(3), 521–527, doi:10.1021/es00052a027.
- Lanz, V. A., M. R. Alfara, U. Baltensperger, B. Buchmann, C. Hueglin, and A. S. H. Prevot (2007), Source apportionment of submicron organic aerosols at an urban site by factor analytical modelling of aerosol mass spectra, *Atmos. Chem. Phys.*, *7*(6), 1503–1522, doi:10.5194/acp-7-1503-2007.
- Lee, J., and D. A. Lane (2009), Unique products from the reaction of naphthalene with the hydroxyl radical, *Atmos. Environ.*, *43*(32), 4886–4893, doi:10.1016/j.atmosenv.2009.07.018.
- Lee, J., and D. A. Lane (2010), Formation of oxidized products from the reaction of gaseous phenanthrene with the OH radical in a reaction chamber, *Atmos. Environ.*, *44*(20), 2469–2477, doi:10.1016/j.atmosenv.2010.03.008.
- Lim, Y. B., and P. J. Ziemann (2005), Products and mechanism of secondary organic aerosol formation from reactions of n-alkanes with OH radicals in the presence of NO<sub>x</sub>, *Environ. Sci. Technol.*, *39*(23), 9229–9236, doi:10.1021/es051447g.
- Lim, Y. B., and P. J. Ziemann (2009), Chemistry of secondary organic aerosol formation from OH radical-initiated reactions of linear, branched, and cyclic alkanes in the presence of NO<sub>x</sub>, *Aerosol Sci. Technol.*, *43*(6), 604–619, doi:10.1080/02786820902802567.
- Liu, B. Y. H., and K. W. Lee (1976), Efficiency of membrane and nucleopore filters for submicrometer aerosols, *Environ. Sci. Technol.*, *10*(4), 345–350, doi:10.1021/es60115a002.
- Liu, S., M. Hu, S. Slanina, L.-Y. He, Y.-W. Niu, E. Brüegemann, T. Gnauk, and H. Herrmann (2008), Size distribution and source analysis of ionic compositions of aerosols in polluted periods at Xinken in Pearl River Delta (PRD) of China, *Atmos. Environ.*, *42*(25), 6284–6295, doi:10.1016/j.atmosenv.2007.12.035.
- Liu, S., S. Takahama, L. M. Russell, S. Gilardoni, and D. Baumgardner (2009), Oxygenated organic functional groups and their sources in single and submicron organic particles in MILAGRO 2006 campaign, *Atmos. Chem. Phys.*, *9*(18), 6849–6863, doi:10.5194/acp-9-6849-2009.
- Liu, S., D. A. Day, J. E. Shields, and L. M. Russell (2011), Ozone-driven daytime formation of secondary organic aerosol containing carboxylic acid groups and alkane groups, *Atmos. Chem. Phys.*, *11*(16), 8321–8341, doi:10.5194/acp-11-8321-2011.
- Liu, S., L. M. Russell, D. T. Sueper, and T. B. Onasch (2012), Organic particle types by single-particle measurements using a time-of-flight aerosol mass spectrometer coupled with a light scattering module, *Atmos. Meas. Tech. Discuss.*, *5*, 3047–3077, doi:10.5194/amtd-5-3047-2012.
- Mader, B. T., R. C. Flagan, and J. H. Seinfeld (2001), Sampling atmospheric carbonaceous aerosols using a particle trap impactor/denuder sampler, *Environ. Sci. Technol.*, *35*(24), 4857–4867, doi:10.1021/es011059o.
- Maria, S. F., L. M. Russell, B. J. Turpin, and R. J. Porcja (2002), FTIR measurements of functional groups and organic mass in aerosol samples over the Caribbean, *Atmos. Environ.*, *36*(33), 5185–5196, doi:10.1016/S1352-2310(02)00654-4.
- Maria, S. F., L. M. Russell, M. K. Gilles, and S. C. B. Myneni (2004), Organic aerosol growth mechanisms and their climate-forcing implications, *Science*, *306*(5703), 1921–1924, doi:10.1126/science.1103491.
- Mohr, C., et al. (2012), Identification and quantification of organic aerosol from cooking and other sources in Barcelona using aerosol mass spectrometer data, *Atmos. Chem. Phys.*, *12*, 1649–1665, doi:10.5194/acp-12-1649-2012.
- Myers, C. O. (1986), Kern River cogeneration project, *IEEE ElectroTechnol. Rev.*, *2*, 113–114.
- Na, K., C. Song, C. Switzer, and D. R. Cocker III (2007), Effect of ammonia on secondary organic aerosol formation from alpha-Pinene ozonolysis in dry and humid conditions, *Environ. Sci. Technol.*, *41*(17), 6096–6102, doi:10.1021/es061956y.
- Nakao, S., M. Shrivastava, N. Anh, H. Jung, and D. R. Cocker III (2011), Interpretation of secondary organic aerosol formation from diesel exhaust photooxidation in an environmental chamber, *Aerosol Sci. Technol.*, *45*(8), 964–972, doi:10.1080/02786826.2011.573510.
- Ng, N. L., et al. (2010), Organic aerosol components observed in Northern Hemispheric datasets from Aerosol Mass Spectrometry, *Atmos. Chem. Phys.*, *10*(10), 4625–4641, doi:10.5194/acp-10-4625-2010.
- Ng, N. L., M. R. Canagaratna, J. L. Jimenez, P. S. Chhabra, J. H. Seinfeld, and D. R. Worsnop (2011), Changes in organic aerosol composition with aging inferred from aerosol mass spectra, *Atmos. Chem. Phys.*, *11*(13), 6465–6474, doi:10.5194/acp-11-6465-2011.
- Offenberg, J. H., M. Lewandowski, M. Jaoui, and T. E. Kleindienst (2011), Contributions of biogenic and anthropogenic hydrocarbons to secondary organic aerosol during 2006 in Research Triangle Park, NC, *Aerosol Air Qual. Res.*, *11*(2), 99–108.
- Paatero, P., and U. Tapper (1994), Positive matrix factorization—A non-negative factor model with optimal utilization of error-estimates of data values, *Environmetrics*, *5*(2), 111–126, doi:10.1002/env.3170050203.
- Pye, H. O. T., and G. A. Pouliot (2012), Modeling the role of alkanes, polycyclic aromatic hydrocarbons, and their oligomers in secondary organic aerosol formation, *Environ. Sci. Technol.*, *46*, 6041–6047, doi:10.1021/es300409w.
- Richard, A., et al. (2011), Source apportionment of size and time resolved trace elements and organic aerosols from an urban courtyard site in Switzerland, *Atmos. Chem. Phys.*, *11*(17), 8945–8963, doi:10.5194/acp-11-8945-2011.
- Richter, H., and J. B. Howard (2000), Formation of polycyclic aromatic hydrocarbons and their growth to soot—A review of chemical reaction pathways, *Prog. Energy Combust. Sci.*, *26*(4–6), 565–608, doi:10.1016/S0360-1285(00)00009-5.
- Rodgers, J. L., and W. A. Nicewander (1988), Thirteen ways to look at the correlation-coefficient, *Am. Stat.*, *42*(1), 59–66, doi:10.2307/2685263.
- Rollins, A. W., et al. (2012), Evidence for NO<sub>x</sub> control over nighttime SOA formation, *Science*, *337*, 1210–1212, doi:10.1126/science.1221520.
- Russell, L. M. (2003), Aerosol organic-mass-to-organic-carbon ratio measurements, *Environ. Sci. Technol.*, *37*(13), 2982–2987, doi:10.1021/es026123w.
- Russell, L. M., S. F. Maria, and S. C. B. Myneni (2002), Mapping organic coatings on atmospheric particles, *Geophys. Res. Lett.*, *29*(16), 1779, doi:10.1029/2002GL014874.
- Russell, L. M., S. Takahama, S. Liu, L. N. Hawkins, D. S. Covert, P. K. Quinn, and T. S. Bates (2009), Oxygenated fraction and mass of organic aerosol from direct emission and atmospheric processing measured on the R/V Ronald Brown during TEXAQS/GoMACCS 2006, *J. Geophys. Res.*, *114*, D00F05, doi:10.1029/2008JD011275.
- Russell, L. M., R. Bahadur, and P. J. Ziemann (2011), Identifying organic aerosol sources by comparing functional group composition in chamber and atmospheric particles, *Proc. Natl. Acad. Sci. U. S. A.*, *108*(9), 3516–3521, doi:10.1073/pnas.1006461108.
- Schade, G. W., and P. J. Crutzen (1995), Emission of aliphatic-amines from animal husbandry and their reactions-potential source of N<sub>2</sub>O and HCN, *J. Atmos. Chem.*, *22*(3), 319–346, doi:10.1007/BF00696641.
- Schauer, J. J., and G. R. Cass (2000), Source apportionment of wintertime gas-phase and particle-phase air pollutants using organic compounds as tracers, *Environ. Sci. Technol.*, *34*(9), 1821–1832, doi:10.1021/es981312t.
- Schauer, J. J., W. F. Rogge, L. M. Hildemann, M. A. Mazurek, G. R. Cass, and B. R. T. Simoneit (1996), Source apportionment of airborne particulate matter using organic compounds as tracers, *Atmos. Environ.*, *30*(22), 3837–3855, doi:10.1016/1352-2310(96)00085-4.
- Schauer, J. J., M. J. Kleeman, G. R. Cass, and B. R. T. Simoneit (1999), Measurement of emissions from air pollution sources. 2. C-1 through C-30 organic compounds from medium duty diesel trucks, *Environ. Sci. Technol.*, *33*(10), 1578–1587, doi:10.1021/es980081n.
- Schauer, J. J., M. P. Fraser, G. R. Cass, and B. R. T. Simoneit (2002a), Source reconciliation of atmospheric gas-phase and particle-phase pollutants during a severe photochemical smog episode, *Environ. Sci. Technol.*, *36*(17), 3806–3814, doi:10.1021/es011458j.
- Schauer, J. J., M. J. Kleeman, G. R. Cass, and B. R. T. Simoneit (2002b), Measurement of emissions from air pollution sources. 5. C-1-C-32 organic compounds from gasoline-powered motor vehicles, *Environ. Sci. Technol.*, *36*(6), 1169–1180, doi:10.1021/es0108077.
- Schwartz, R. E., et al. (2010), Biogenic oxidized organic functional groups in aerosol particles from a mountain forest site and their similarities to laboratory chamber products, *Atmos. Chem. Phys.*, *10*(11), 5075–5088, doi:10.5194/acp-10-5075-2010.
- Seinfeld, J. H., and S. N. Pandis (2006), *Atmospheric Chemistry and Physics—From air Pollution to Climate Change*, John Wiley, Hoboken, N. J.

- Shakya, K. M., and R. J. Griffin (2010), Secondary organic aerosol from photooxidation of polycyclic aromatic hydrocarbons, *Environ. Sci. Technol.*, *44*(21), 8134–8139, doi:10.1021/es1019417.
- Sheesley, R. J., J. J. Schauer, and D. Kenski (2004), Trends in secondary organic aerosol at a remote site in Michigan's Upper Peninsula, *Environ. Sci. Technol.*, *38*, 6491–6500, doi:10.1021/es049104q.
- Sorooshian, A., S. N. Murphy, S. Hersey, H. Gates, L. T. Padro, A. Nenes, F. J. Brechtel, H. Jonsson, R. C. Flagan, and J. H. Seinfeld (2008), Comprehensive airborne characterization of aerosol from a major bovine source, *Atmos. Chem. Phys.*, *8*(17), 5489–5520, doi:10.5194/acp-8-5489-2008.
- Srivastava, A., S. Gupta, and V. K. Jain (2008), Source apportionment of total suspended particulate matter in coarse and fine size ranges over Delhi, *Aerosol Air Qual. Res.*, *8*(2), 188–200.
- Stein, S. E., and D. R. Scott (1994), Optimization and testing of mass-spectral library search algorithms for compound identification, *J. Am. Soc. Mass Spectrom.*, *5*(9), 859–866, doi:10.1016/1044-0305(94)87009-8.
- Sun, Y. L., et al. (2011), Characterization of the sources and processes of organic and inorganic aerosols in New York City with a high-resolution time-of-flight aerosol mass spectrometer, *Atmos. Chem. Phys.*, *11*(4), 1581–1602, doi:10.5194/acp-11-1581-2011.
- Surratt, J. D., et al. (2008), Organosulfate formation in biogenic secondary organic aerosol, *J. Phys. Chem. A*, *112*(36), 8345–8378, doi:10.1021/jp802310p.
- Takahama, S., S. Gilardoni, L. M. Russell, and A. L. D. Kilcoyne (2007), Classification of multiple types of organic carbon composition in atmospheric particles by scanning transmission X-ray microscopy analysis, *Atmos. Environ.*, *41*(40), 9435–9451, doi:10.1016/j.atmosenv.2007.08.051.
- Takahama, S., S. Liu, and L. M. Russell (2010), Coatings and clusters of carboxylic acids in carbon-containing atmospheric particles from spectro-microscopy and their implications for cloud-nucleating and optical properties, *J. Geophys. Res.*, *115*, D01202, doi:10.1029/2009JD012622.
- Tanner, R. L., and B. Zielinska (1994), Determination of the biogenic emission rates of species contributing to VOC in the San Joaquin Valley of California, *Atmos. Environ.*, *28*(6), 1113–1120, doi:10.1016/1352-2310(94)90288-7.
- Tegen, I., and A. A. Lacis (1996), Modeling of particle size distribution and its influence on the radiative properties of mineral dust aerosol, *J. Geophys. Res.*, *101*(D14), 19,237–19,244, doi:10.1029/95JD03610.
- Tivanski, A. V., R. J. Hopkins, T. Tylliszczak, and M. K. Gilles (2007), Oxygenated interface on biomass burn tar balls determined by single particle scanning transmission X-ray microscopy, *J. Phys. Chem. A*, *111*(25), 5448–5458, doi:10.1021/jp070155u.
- Turpin, B. J., J. J. Huntzicker, S. M. Larson, and G. R. Cass (1991), Los Angeles summer midday particulate carbon-primary and secondary aerosol, *Environ. Sci. Technol.*, *25*(10), 1788–1793, doi:10.1021/es00022a017.
- Turpin, B. J., P. Saxena, and E. Andrews (2000), Measuring and simulating particulate organics in the atmosphere: Problems and prospects, *Atmos. Environ.*, *34*(18), 2983–3013, doi:10.1016/S1352-2310(99)00501-4.
- Ulbrich, I. M., M. R. Canagaratna, Q. Zhang, D. R. Worsnop, and J. L. Jimenez (2009), Interpretation of organic components from Positive Matrix Factorization of aerosol mass spectrometric data, *Atmos. Chem. Phys.*, *9*(9), 2891–2918, doi:10.5194/acp-9-2891-2009.
- Ulbrich, I. M., M. R. Canagaratna, M. J. Cubison, Q. Zhang, N. L. Ng, A. C. Aiken, and J. L. Jimenez (2012), Three-dimensional factorization of size-resolved organic aerosol mass spectra from Mexico City, *Atmos. Meas. Tech.*, *5*, 195–224, doi:10.5194/amt-5-195-2012.
- Usher, C. R., A. E. Michel, and V. H. Grassian (2003), Reactions on mineral dust, *Chem. Rev.*, *103*(12), 4883–4940, doi:10.1021/cr020657y.
- Wallace, L. A., S. J. Emmerich, and C. Howard-Reed (2004), Source strengths of ultrafine and fine particles due to cooking with a gas stove, *Environ. Sci. Technol.*, *38*(8), 2304–2311, doi:10.1021/es0306260.
- Wang, L., R. Atkinson, and J. Arey (2007), Dicarbonyl products of the OH radical-initiated reactions of naphthalene and the C-1- and C-2-alkylnaphthalenes, *Environ. Sci. Technol.*, *41*(8), 2803–2810, doi:10.1021/es0628102.
- Wängberg, I., I. Barnes, and K. H. Becker (1997), Product and mechanistic study of the reaction of NO<sub>3</sub> radicals with alpha-pinene, *Environ. Sci. Technol.*, *31*(7), 2130–2135, doi:10.1021/es960958n.
- Ward, J. H. (1963), Hierarchical grouping to optimize an objective function, *J. Am. Stat. Assoc.*, *58*(301), 236–244, doi:10.1080/01621459.1963.10500845.
- Webb, P. J., J. F. Hamilton, A. C. Lewis, and K. Wirtz (2006), Formation of oxygenated-polycyclic aromatic compounds in aerosol from the photo-oxidation of o-tolualdehyde, *Polycyclic Aromatic Compounds*, *26*(4), 237–252, doi:10.1080/07352680600903932.
- Whitby, K. T., B. Y. H. Liu, and R. B. Husar (1972), Aerosol size distribution of Los Angeles smog, *J. Colloid Interface Sci.*, *39*(1), 177–204, doi:10.1016/0021-9797(72)90153-1.
- Williams, B. J., A. H. Goldstein, N. M. Kreisberg, and S. V. Hering (2006), An in-situ instrument for speciated organic composition of atmospheric aerosols: Thermal Desorption Aerosol GC/MS-FID (TAG), *Aerosol Sci. Technol.*, *40*(8), 627–638, doi:10.1080/02786820600754631.
- Worton, D. R., et al. (2011), Origins and composition of fine atmospheric carbonaceous aerosol in the Sierra Nevada Mountains, California, *Atmos. Chem. Phys.*, *11*(19), 10,219–10,241, doi:10.5194/acp-11-10219-2011.
- Yee, L. D., J. S. Craven, C. L. Loza, K. A. Schilling, N. L. Ng, M. R. Canagaratna, P. J. Ziemann, R. C. Flagan, and J. H. Seinfeld (2012), Secondary organic aerosol formation from low-NO<sub>x</sub> photooxidation of dodecane: Evolution of multi-generation gas-phase chemistry and aerosol composition, *J. Phys. Chem. A*, *116*, 6211–6230, doi:10.1021/jp211531h.
- Zhang, H., J. D. Surratt, Y. H. Lin, J. Bapat, and R. M. Kamens (2011), Effect of relative humidity on SOA formation from isoprene/NO photooxidation: Enhancement of 2-methylglyceric acid and its corresponding oligoesters under dry conditions, *Atmos. Chem. Phys.*, *11*(13), 6411–6424, doi:10.5194/acp-11-6411-2011.
- Zhang, Q., M. R. Canagaratna, J. T. Jayne, D. R. Worsnop, and J. L. Jimenez (2005), Time- and size-resolved chemical composition of submicron particles in Pittsburgh: Implications for aerosol sources and processes, *J. Geophys. Res.*, *110*, D07S09, doi:10.1029/2004JD004649.
- Zhang, Q., et al. (2007), Ubiquity and dominance of oxygenated species in organic aerosols in anthropogenically influenced Northern Hemisphere mid-latitudes, *Geophys. Res. Lett.*, *34*, L13801, doi:10.1029/2007GL029979.
- Zheng, M., G. R. Cass, J. J. Schauer, and E. S. Edgerton (2002), Source apportionment of PM<sub>2.5</sub> in the southeastern United States using solvent-extractable organic compounds as tracers, *Environ. Sci. Technol.*, *36*(11), 2361–2371, doi:10.1021/es011275x.
- Zhong, S. Y., C. D. Whiteman, and X. D. Bian (2004), Diurnal evolution of three-dimensional wind and temperature structure in California's Central Valley, *J. Appl. Meteorol.*, *43*(11), 1679–1699, doi:10.1175/JAM2154.1.